GPO PRICE $ _____

OTS PRICE(S) $ _____

Hard copy (HC) _____

Microfiche (MF) _____

TECHNICAL MEMORANDUM

X-374

EFFECTS OF WING INCIDENCE ON THE LONGITUDINAL

TRIM CHARACTERISTICS OF A CAMBERED 70°

DELTA-WING CONFIGURATION AT MACH

NUMBERS FROM 3.0 TO 5.0

By Warren F. Ahtye

Ames Research Center
Moffett Field, Calif.

NATIONAL AERONAUTICS AND SPACE ADMINISTRATION

WASHINGTON   September 1960

NATIONAL AERONAUTICS AND SPACE ADMINISTRATION

TECHNICAL MEMORANDUM X-374

EFFECTS OF WING INCIDENCE ON THE LONGITUDINAL

TRIM CHARACTERISTICS OF A CAMBERED 70°

DELTA-WING CONFIGURATION AT MACH

NUMBERS FROM 3.0 TO 5.0*

By Warren F. Ahtye

SUMMARY

Tests were conducted at Mach numbers from 3.0 to 5.0 on a delta-wing and body configuration to determine the effect of wing camber and incidence on the trim characteristics of the configuration. It was found that for an assumed moment reference which insures static longitudinal stability from subsonic speeds up to a Mach number of 5.0, the combined use of incidence and camber is required to trim the configuration at the attitude for maximum lift-drag ratio. The attendant loss in the maximum lift-drag ratio was 10 percent and is attributed entire to the effect of camber. If a reference moment center were chosen so that static longitudinal stability existed up to a Mach number of 3.0 only, then the trim requirements would be less stringent. As a result through the use of only the limited incidence tested, the configuratio could be trimmed at a Mach number of 3.0 with no loss in maximum lift-drag ratio. The variations of longitudinal trim characteristics with camber and incidence for this delta-wing configuration were accurately predicted by simple linear theories described in this report.

INTRODUCTION

An important requirement for efficient flight, especially at supersonic speeds, is that of trimming an airplane at the attitude for maximum lift-drag ratio with a minimum trim-drag penalty. A promising method available for supplying trim moment at supersonic speeds is the use of negative wing incidence. In references 1 and 2 it was indicate theoretically and experimentally for various delta wings that limited

---

*Title Unclassified

amounts of negative incidence produced sizable trim moments with no decrease in the maximum lift-drag ratio (i.e., no trim drag penalty) at low supersonic speeds. Additional trim moment can be obtained through the use of wing section camber.

The primary purposes of this report are: (1) to present test results on the effect of negative wing incidence on the performance and static stability characteristics of a delta-wing configuration at higher Mach numbers than those previously reported, (2) to present test results on the effects of an asymmetric airfoil section at these higher Mach numbers, and (3) to establish the validity of theoretical methods for the prediction of the effect of wing camber and incidence on the longitudinal trim characteristics of similar delta-wing configurations.

SYMBOLS

$\bar{a}$ distance from moment center to exposed wing center of area, in.

A axial force, lb

b wing span, in.

$\bar{c}$ wing mean aerodynamic chord, in.

c_r wing root chord, in.

C_A axial force coefficient, $\dfrac{A}{qS}$

C_D drag coefficient, $\dfrac{D}{qS}$

C_L lift coefficient, $\dfrac{L}{qS}$

C_{L_0} lift coefficient at zero angle of attack

C_{l_β} rate of change of rolling-moment coefficient, $\dfrac{\text{rolling moment}}{qSb}$, with angle of sideslip at zero sideslip, per deg

C_m pitching-moment coefficient, $\dfrac{\text{pitching moment}}{qSc_r}$

ΔC_m incremental pitching-moment coefficient due to camber or incidence

C_{n_β} rate of change of yawing-moment coefficient, $\dfrac{\text{yawing moment}}{qSb}$, with angle of sideslip at zero sideslip, per deg

C_{Y_β} rate of change of side-force coefficient, $\dfrac{\text{side force}}{qS}$, with angle of sideslip at zero sideslip, per deg

D drag, lb

i_w wing incidence angle, radians

L lift, lb

M free-stream Mach number

q free-stream dynamic pressure, lb/sq in.

S total wing area including area blanketed by the fuselage, in.^{2}

x body station measured from the nose, in.

α angle of attack of body center line, radians (unless otherwise specified)

α_w angle of attack of wing plane, radians (unless otherwise specified)

γ ratio of specific heat at constant pressure to specific heat at constant volume

δ surface deflection angle, radians

Subscripts

a asymmetric

α rate of change with angle of attack, per radian (unless otherwise specified)

B body alone

B(W) body in presence of wing

C combination

cam due to camber

cg center of gravity

d compression region

e   expansion region

EW   effective wing

I   interference quantity

L   due to lift

max   maximum

o   conditions at zero lift (except C_{L_o} and C_{N_o})

s   symmetric

W   exposed wing alone

W(B)   wing in the presence of body

MODELS

The sketches of figure 1 show the four wing-body combinations which were tested. All four models used identical delta wings of half-diamond airfoil section, and differed only in wing incidence and afterbody shape. The wing of the 0° incidence model (fig. 1(a)) was mounted near the center line of the body of revolution. The wings of the -3° incidence model (fig. 1(c)) and both -6° incidence models (figs. 1(b) and 1(d)) were mounted so that the trailing edges of the wings were located as close as possible to the top of the bodies.

The fuselages for all four models are essentially half-power bodies of revolution (see fig. 1). The 0° model and a -6° incidence model utilized this basic half-power body without modification. For the -3° and the other -6° incidence models sufficient volume was added to the basic body at the lower fuselage-wing juncture to maintain the maximum fuselage width from the body reference plane up to the lower wing surface. The modification resulted in a 1.5 percent increase in body volume for the -6° incidence model and a 2.4 percent increase for the -3° incidence model. The modified -3° incidence body required more added volume because the entire wing was above the body reference plane. For the modified bodies the cross-section area below the wing increased with increasing distance aft; thus one of the requirements for favorable lift interference (ref. 3) was satisfied.

The vertical location of the moment reference center lies in the body reference plane. The longitudinal location of the moment reference center is at 32.5 percent of the wing mean aerodynamic chord and is forward of the wing center of area by approximately 12 percent of the wing root chord. This particular moment reference was chosen so that the least stable model would have positive static margins at

normal flight conditions from subsonic speeds up to the maximum test
Mach number. Test results for a model with similar wing plan form
(ref. 4) were used to estimate the stability levels of these models
at Mach numbers below 3.0.

APPARATUS AND TESTS

The tests were conducted in the 10- by 14-inch supersonic wind
tunnel at Mach numbers of 3.0, 4.0, and 5.0. For a description of the
10- by 14-inch wind tunnel see reference 5. Forces and moments on the
models were measured with a six-component, strain-gage balance located
immediately aft of the base of the test models. Measurements were made
at angles of attack from -4° to $+11^O$, and sideslip angles from -4° to
$+4^O$ at several angles of attack.

The axial force has been adjusted for the difference between the
base and the free-stream static pressure.

The normal and axial force data were converted to wind axes to
obtain C_L and C_D. The pitching, yawing, and rolling moments, and
the side forces were retained in body axes. The directional and
lateral data were plotted relative to sideslip angle, β, and the
derivatives C_{Y_β}, C_{n_β}, and C_{l_β} were evaluated from the plots.

Wind-tunnel calibration data were employed in combination with
stagnation pressure measurements to obtain the stream static and
dynamic pressures. Test Reynolds numbers based on the root chord
of the model wing were as follows:

Mach number	Reynolds number, millions
3.0	3.2
4.0	4.5
5.0	2.1

ACCURACY OF TEST RESULTS

The accuracy of test results was influenced by uncertainties in
the measurements of forces and moments and in the determination of
stream static and dynamic pressures and angles of attack and sideslip.
The uncertainties resulted in estimated probable errors in the test
results as shown in the following table:

Parameter	M=3.0	M=4.0	M=5.0
M	±0.01	±0.03	±0.03
C_L	$\pm.002$	$\pm.002$	$\pm.002$
C_D	$\pm.0002$	$\pm.0003$	$\pm.0005$
L/D	$\pm.05$	$\pm.05$	$\pm.10$
C_m	$\pm.0004$	$\pm.0004$	$\pm.0006$
C_{Y_β}, per deg	$\pm.0001$	$\pm.0002$	$\pm.0004$
C_{n_β}, per deg	$\pm.00002$	$\pm.00004$	$\pm.00008$
C_{l_β}, per deg	$\pm.00004$	$\pm.00006$	$\pm.00008$
α, deg	$\pm.1$	$\pm.1$	$\pm.1$

RESULTS AND DISCUSSION

Effect of Camber and Incidence

The primary longitudinal data for the basic body alone, the 0° incidence model in the upright and inverted positions (i.e., flat side of wing facing up and down, respectively), and the -6° incidence model are presented in figures 2 and 3. The effects of wing camber and incidence on longitudinal characteristics, shown in figures 4 to 6, were determined from these data. The effect of incidence can be seen by a direct comparison of the longitudinal data for the 0° incidence model in the upright position and for the -6° incidence model with the symmetrical body. However, the effect of section camber on the stability and performance characteristics of the 0° incidence configuration cannot be obtained directly from the primary data. The camber effect could be obtained by direct comparison with the characteristics for a similar configuration with a symmetric (diamond) airfoil of the same chordwise thickness distribution. Since a configuration with a symmetric airfoil was not tested, the longitudinal characteristics were estimated by averaging the test results at a constant angle of attack for the existing 0° incidence model with the asymmetric airfoil in the upright and inverted positions (figs. 2 and 3). All longitudinal parameters, with the exception of zero-lift drag, were obtained in this manner. The justification of the averaging process is discussed in appendix A. The zero-lift drag for the model with a symmetric airfoil was obtained by subtracting a theoretical increment due to camber from the experimental zero-lift drag for the model with the asymmetrical airfoil. The linearized conical flow theory of reference 6 was used for this purpose.

In the remainder of this discussion the 0° incidence model with an asymmetric airfoil (half diamond with flat side up) will be referred to as the "asymmetric model" and the 0° incidence model with a symmetric airfoil of equal thickness will be referred to as the "symmetric model."

Longitudinal trim and performance characteristics.- Figures 4 to 6 summarize the effect of camber and incidence on longitudinal characteristics. The component moments are presented in figure 4 as a ratio of the pitching-moment increment due to camber and/or incidence to the pitching moment required to trim the symmetric model. The ratio is taken at the average lift coefficient for maximum lift-drag ratio. For the assumed moment center, the pitching moment due to incidence supplied a large part of the pitching moment required to trim the configuration. This incidence contribution consists of two parts: (1) the zero-lift pitching moment which stems from positive lift on the nose of the body and negative lift in the vicinity of the wing center of area, and (2) an incremental moment due to the decrease in stability as the lift coefficient increases from zero up to the value where the maximum lift-drag ratio is attained. The zero-lift moment forms the largest part of the incidence moment. The total incidence moment shown in figure 4 increases with increasing Mach number. This variation is attributed to the decrease in stability with increasing Mach number (fig. 6).

The pitching moment due to camber at a Mach number of 3.0 is of the same order of magnitude as that due to incidence. However, the camber moment decreases with increasing Mach number and is relatively small at a Mach number of 5.0. By use of the two-dimensional airfoil theory (second-order approximation) as described in appendix A, it is predicted that the value of the $\Delta C_m/C_{m_S}$ ratio in figure 4 is approximately constant for the moment due to camber. The reason for the anomalous drop-off of the experimental camber moment is not readily apparent. It is seen in figure 4 that the combined use of camber and the limited incidence tested is necessary at all test Mach numbers to trim the configuration at the lift coefficient for maximum lift-drag ratio.

The effect of wing camber and incidence on the maximum lift-drag ratio is seen in figure 5. The substitution of an asymmetric airfoil for a symmetric airfoil of the same thickness (2.5 percent) in order to supply trim moment results in a loss of approximately 10 percent in the maximum lift-drag ratio throughout the test Mach number range. This change can be attributed to a positive value of the term $(C_{A_\alpha} - C_{L_o})$ and to an increase in the wing wave drag, which are discussed in appendix A. The effect of each of these two factors can be seen in figure 5 by comparing the lift-drag ratio for the symmetric and asymmetric models with the average lift-drag ratio for the upright and inverted runs. The latter represents the lift-drag ratio for a model with the zero-lift drag of the asymmetric model but with the drag-due-to-lift characteristics of the symmetric model. Each effect results in a loss of approximately 5 percent in the maximum lift-drag ratio

throughout the Mach number range. Figure 5 also shows that 6° of
negative wing incidence does not affect the values of maximum lift-
drag ratio at Mach numbers of 3.0 and 4.0, and slightly decreases the
maximum lift-drag ratio at a Mach number of 5.0. The small trim drag
penalty due to incidence at a Mach number of 5.0 is believed to be
due to a movement of the boundary-layer transition point on the body.
The approximate magnitude of this effect is shown in appendix B.

The effect of camber and incidence on the static longitudinal
stability of the configuration can be seen in figures 2 and 6. Compari-
son of the results for a symmetric and the asymmetric model shows that
camber has no effect on stability, as predicted by the two-dimensional
airfoil theory of appendix A.

The effect of incidence can be seen in the comparison of the
stability of the 0° incidence model in the upright position with that
of the -6° incidence model. At zero lift coefficient the levels of
stability are approximately the same for both models (fig. 2). The use
of 6° of negative wing incidence results in a decrease in stability at
higher lift coefficients. At a Mach number of 3.0 the decrease in
static margin is approximately 2.5 percent of the mean aerodynamic
chord at the lift coefficient for maximum lift-drag ratio. At a Mach
number of 5.0 the decrease amounts to 7 percent of the mean aerodynamic
chord. Negative incidence causes a decrease in stability with increas-
ing lift coefficient due to the nonlinearity of the body-alone lift
curve. At a given lift coefficient the body of the incidence model is
at a higher angle of attack and carries a more than proportionate
amount of the total lift. This effect becomes more pronounced at higher
Mach numbers as the lift-curve slope for the isolated wing decreases
with Mach number while that for the body alone remains constant (fig. 7).

It has been shown that in the Mach number range from 3.0 to 5.0,
the combined use of camber and the limited incidence tested is required
to trim the configuration at the attitude for maximum lift-drag ratio.
The attendant loss in the maximum lift-drag ratio was approximately 10
percent. It was estimated that sufficient static longitudinal stability
existed for the configuration with incidence and camber from subsonic
speeds up to a Mach number of 5.0, with the least stable flight condi-
tion occurring at the highest Mach number. As a result, this flight
condition dictated the location of the moment reference center.

If the maximum speed of this configuration were limited to a Mach
number of 3.0, the location of the reference moment center would then
be dictated by the stability requirements at this flight condition.
Examination of the static longitudinal characteristics at a Mach number
of 3.0 (fig. 2(a)) shows that a rearward movement of 5-percent mean
aerodynamic chord (3.3 percent of root chord) of the reference moment
center to lessen the trim requirements still leaves sufficient static

A
2
2
4

A
2
2
4

longitudinal stability. It is also estimated that sufficient static longitudinal stability would exist at subsonic speeds. With the moment center at $37.5\bar{c}$, the configuration may be trimmed near the attitude for maximum lift-drag ratio through the use of -6° wing incidence alone with essentially no decrease in the maximum lift-drag ratio.

Comparison of theoretical and experimental results.- The lift, pitching moment (with the exception of moment due to camber), and drag due to lift, for the 0° incidence model in the upright position, the -6° incidence model, and the body alone have been estimated by simple theoretical methods, and are compared with the experimental data in figures 8 to 12. The purpose of these comparisons is to determine the validity of the theoretical methods for the prediction of the effects of wing camber and incidence on the longitudinal characteristics of similar delta-wing configurations. The procedures are found in appendices A and B.

The predicted and experimental lifts are compared in figure 8 for the body alone, the 0° incidence model in the upright position, and the -6° incidence model with the symmetrical body. The body-alone prediction is accurate for the lift-curve slope at zero angle of attack. The agreement of predicted and experimental values is only fair at angles of attack greater than 5°. The values of lift predicted for the 0° and -6° incidence models agree well with the experimental values in all cases. It should be noted that for the -6° incidence model agreement of the lifts, which are composed largely of interference lift, indicates that the interference lift is accurately predicted.

The predicted values of body-alone pitching moment are compared with experimental values in figure 9, and the approximated pitching moments for the 0° and -6° incidence models are compared with measured moments in figure 10. The theory of reference 7 provides accurate estimations of the body-alone pitching moments up to the highest angle of attack tested. The estimated center-of-pressure locations for the 0° and -6° incidence models are within 1.5 percent $\bar{c}$ of the experimental values, with the exception of the data for the 0° incidence model at a Mach number of 3.0. At this particular condition the large difference can be attributed to the simplifying assumption that the center of pressure of the isolated wing lift acts at the center of area of the exposed wing. The center-of-pressure location estimated by the method of reference 8 results in a much better correlation of experimental and predicted values (appendix B). However, the general agreement of the predicted values with experimental values indicates that the above assumption is sufficiently accurate in the present report to describe the variations in pitching-moment characteristics with wing incidence.

In figure 11 are shown comparisons of the experimental drag coefficient of the body alone with a drag coefficient based on the

slender-body value of the inclination angle. At Mach numbers of 3.0
and 4.0 the experimental variation of drag coefficient with angle of
attack agrees exactly with the α/2 inclination assumption up to
moderate angles of attack (6°). At higher angles, the experimental
values deviate slightly from the predicted variation. Reference 7
ascribes such variance to the increased body crossflow effect. At a
Mach number of 5.0 the values of experimental and estimated drag
coefficient for the body alone are not in good agreement. The exist-
ence of a discontinuity in C_{D_α} at zero angle of attack indicates
movement of the boundary-layer transition point on the nose of the
body, which accounts for the discrepancy.

The predicted drag polars for the 0° and -6° incidence configura-
tions are compared with the corresponding experimental drag polars in
figure 12. The predicted polars were obtained by adding the predicted
drag due to lift (appendix B) and the predicted drag due to camber
(appendix A) to the experimental zero-lift drag for the 0° incidence
model in the upright position. At Mach numbers of 3.0 and 4.0 the
agreement is fairly good, with the predicted drag due to lift slightly
lower than the experimental value. The differences can be attributed
to two effects: (1) an underestimation of the effective inclination
angle of body-alone lift at the higher angles of attack (fig. 11), and
(2) an underestimation of lift of the body alone at the higher angles
of attack (fig. 8). Verification of this statement lies in the fact
that the difference between the calculated and experimental body-alone
drag due to lift (fig. 11) is of the same magnitude as the difference
in drag for the 0° incidence model (fig. 12). The comparisons at Mach
numbers of 3.0 and 4.0 indicate that the remaining drag-due-to-lift
components are accurately determined by use of the assumed inclinations
of these lifts. At a Mach number of 5.0 there is a large discrepancy
between the experimental and predicted values of the drag coefficient,
expecially at higher angles of attack. However, it is felt that this
is due to the aforementioned movement of the boundary-layer transition
point on the body. It can be shown from this comparison of the pre-
dicted drags for the 0° and -6° incidence models that a predicted
maximum lift-drag-ratio variation with Mach number shows no incidence
effects.

Lateral-directional characteristics.- The variations of the side-
force, yawing-moment, and rolling-moment derivatives with angle of
attack are shown in figure 13 for the modified -3° and -6° incidence
models and the 0° incidence model. The effect of incidence on the
lateral-directional characteristics can be seen from a comparison of
the derivatives for the 0°, and the modified -3° and -6° incidence
models. (It is assumed that the fuselage modification does not affect
the lateral-directional characteristics.) The results shown in figure
13 indicate that variations in wing incidence have very little effect
on the static directional stability. However, the static lateral

stability as plotted in figure 13 varies with both angle of attack and angle of incidence in no consistent manner.

Effect of Fuselage Modification

One of the requirements for favorable lift interference at positive wing angles of attack calls for a proportioning of the body so that the body cross-sectional area below the wing increases with increasing length (ref. 3). Volume was added to the lower afterbody of the -3° and -6° incidence models in an attempt to improve further the wing-body interference without significant drag increase. The added volume was proportioned so that the incremental cross-sectional area increased with increasing length. The modifications are shown in figures 1(c) and 1(d) and described in the "model" section.

The effect of the modification to the fuselage of the -6° incidence model can be seen in figures 14 and 15. At small angles of attack no effect on lift and pitching moment is apparent as the filled-in volume is on the lee side of the wing. At angles of attack greater than 8°, where the filled-in volume becomes exposed to the free stream, the lift and static longitudinal stability increase slightly. This increased lift and stability indicates that a small favorable pressure field (i.e., lift increase) does exist in the region of the wing adjacent to the filled-in volume.

The favorable pressure field is attained by the addition of a small amount of body volume (approximately 2 percent). The effect of this added volume is reflected in a slight increase of zero-lift drag (fig. 15(a)). However, little decrease in the maximum lift-drag is apparent as the magnitude of the favorable pressure field is sufficient to compensate performancewise for the increased zero-lift drag.

The data for the -3° incidence model are also shown in figures 14 and 15. The added volume (3 percent) and the resulting change in body contour are greater than those for the -6° incidence model. Despite the larger body volume, the maximum lift-drag ratio for the -3° incidence model is approximately the same as for the -6° incidence model.

CONCLUSIONS

Tests were performed in the Ames 10- by 14-inch supersonic wind tunnel at Mach numbers from 3.0 to 5.0 to determine the effect of an asymmetrical airfoil section (i.e., camber) and negative wing incidence

on the longitudinal trim, stability, and performance characteristics of a delta-wing and body combination. The results of these tests have led to the following general conclusions:

1. For an assumed moment reference center which insures static longitudinal stability throughout the Mach number range the combined use of incidence and camber is required to trim the configuration at the attitude for maximum lift-drag ratio, with an attendant loss of 10 percent in the maximum lift-drag ratio. This loss can be attributed almost entirely to the effect of section camber.

2. If the maximum speed of this configuration were limited to a Mach number of 3.0, the less stringent stability requirements would allow the reference moment center to be moved back. For this assumed reference moment center, the use of incidence alone is sufficient to trim the configuration at the attitude for maximum lift-drag ratio, with no decrease in the maximum lift-drag ratio.

3. The agreement of the predicted values of lift and pitching moment with the experimental values indicates that the simple theories described in this report are sufficient to predict accurately the longitudinal trim characteristics of similar delta-wing configurations utilizing this type of camber and incidence. The method for predicting drag due to lift, although not accurate to the same degree, is still adequate.

Ames Research Center
    National Aeronautics and Space Administration
        Moffett Field, Calif., June 6, 1960

APPENDIX A

THEORETICAL EVALUATION OF THE EFFECTS OF CAMBER

The effects of airfoil section camber on the longitudinal charac-
teristics of the 0° incidence model can be obtained only by comparing
the characteristics of the model utilizing a cambered airfoil with one
utilizing a symmetric airfoil of the same thickness distribution. As
a symmetric airfoil model was not tested, the longitudinal character-
istics were obtained in this report by averaging the test results for
the existing 0° incidence model in the upright and inverted positions.
All longitudinal parameters, with the exception of wave drag at zero
angle of attack were obtained in this manner. The main purpose of this
section is to determine the validity of the "averaging" process. In
addition, the computed aerodynamic terms due to camber will be examined
to determine their effect on the performance characteristics of the
configuration.

LONGITUDINAL CHARACTERISTICS

Two-dimensional airfoil characteristics can be derived from
Busemann's two-dimensional theory. The pressure change through an
oblique shock wave created by deflecting a supersonic stream of air
through a deflection angle of θ is expressed in terms of the first-
and second-order terms as:

where

$$\frac{\Delta p}{q} = G_1\theta + G_2\theta^2 \qquad\qquad (A1)$$
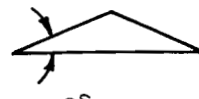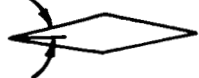
$$G_1 = \frac{2}{\sqrt{M^2 - 1}} \qquad\qquad (A2)$$

$$G_2 = \frac{\gamma M^4 + (M^2 - 2)^2}{2(M^2 - 1)^2} \qquad\qquad (A3)$$

where G denotes the dimensionless constant for series expansion of
the pressure coefficient.

The pertinent two-dimensional characteristics derived from equa-
tion (A1) expressed as the first- and second-order terms are tabulated
below:

Two-Dimensional Airfoil Characteristics

Longitudinal coefficient	$\delta_a = 2\delta_s$	$\delta_a = 2\delta_s$	δ_s
C_{N_0}	$G_2 \delta_a^{\,2}$	$-G_2 \delta_a^{\,2}$	0
$(C_A)_{\alpha=0}$	$G_1 \delta_a^{\,2}$	$G_1 \delta_a^2$	$2G_1 \delta_s^{\,2} = \frac{1}{2} G_1 \delta_a^{\,2}$
$(C_m)_{\alpha=0}$*	$\frac{1}{4} G_1 \delta_a$	$-\frac{1}{4} G_1 \delta_a$	0
C_{N_α}	$2G_1$	$2G_1$	$2G_1$
C_{A_α}	$2G_2 \delta_a^{\,2}$	$-2G_2 \delta_a^{\,2}$	0
C_{m_α}*	$\frac{1}{2} G_2 \delta a$	$\frac{1}{2} G_2 \delta a$	$G_2 \delta_s = \frac{1}{2} G_2 \delta a$

*Moment about mid-chord point.

The tabulation shows that with the exception of wave drag at zero angle
of attack, all longitudinal parameters for the symmetric airfoil may
be obtained, to the second order, by averaging the longitudinal
characteristics for the upright and inverted asymmetric airfoils at a
given angle of attack. Use of the terms of order higher than the
second degree did not always follow the "averaging" variation. Within
the accuracy of the data of this report it was found that the longi-
tudinal characteristics of the symmetric airfoil, exclusive of wave
drag, could be represented by the average of the characteristics for
the upright and inverted airfoil.

PERFORMANCE CHARACTERISTICS

The effect of some of the camber terms in the table on performance can be seen in the following expression for the maximum lift-drag ratio if C_{L_O} and C_{L_α} are taken as C_{N_O} and C_{N_α}, respectively:

$$\left(\frac{L}{D}\right)_{max} = \frac{C_{L_\alpha}}{2\sqrt{-C_{L_O}C_{A_\alpha} + C_{L_\alpha}C_{D(\alpha=0°)}} - C_{L_O} + C_{A_\alpha}} \tag{A6}$$

The use of the cambered airfoil in the upright position to supply trim moment introduces changes in three aerodynamic parameters which affect the maximum lift-drag ratio. These changes are:

1. The appearance of an increasing chord force with angle of attack due to noncancellation of a second-order cross-product term $G_2 \alpha \delta$.

2. The appearance of a positive lift at zero angle of attack due to noncancellation of top and bottom pressures on the airfoil.

3. An increase in the wing wave drag due to the larger stream deflection for the cambered airfoil.

For the configurations described in this report, the product of C_{L_O} and C_{A_α} is insignificant compared to the magnitude of the $C_{L_\alpha} \times C_{D_O}$ term. However, the C_{L_O} and C_{A_α} terms outside of the radical sign in equation (A6) have a significant effect.

The effect of a positive C_{L_O} is to increase the maximum lift-drag ratio, whereas the positive C_{A_α} tends to decrease the maximum lift-drag ratio. For this asymmetric configuration the C_{A_α} term predominates, and the net effect of C_{L_O} and C_{A_α} is a decrease in the maximum lift-drag ratio. The decrease in the maximum lift-drag ratio due to the increase in C_{D_O} resulting from the asymmetry is of the same magnitude.

The magnitudes of the experimental C_A are shown in figure 16 for the asymmetric model in the upright and inverted positions. The estimated values for the upright and inverted two-dimensional asymmetric airfoils are also shown. By the two-dimensional airfoil theory, the C_{A_α} for the symmetric model can be obtained by averaging the C_{A_α} for the upright and inverted asymmetric models. At Mach numbers of 3.0 and 4.0 the experimental data show the same trends. That is, the symmetric model would have zero change of C_A with angle of attack (to the second-order degree of accuracy), whereas the model with camber

has an increasing C_A with increasing angle of attack. At a Mach number of 5.0 the level of the experimental C_{A_α} increases sharply for both the upright and inverted asymmetric models, whereas two-dimensional airfoil theory predicts no radical change in C_{A_α} from Mach number 4.0 to 5.0. This discrepancy can be attributed to a movement of the boundary-layer transition point on the body as discussed earlier.

A
2
2
4

APPENDIX B

THEORETICAL PREDICTION OF THE EFFECTS OF INCIDENCE

Analysis of the results presented in the report has been based on the assumption that all the effects of incidence can be attributed to the change in the relative loads on the body and wing at a given lift coefficient. The theoretical method of reference 8 was used to separate the configuration lift for the 0° and -6° incidence models into component lifts, and to determine the centers of pressure and angles of inclination of the component forces. The relations between the change in wing incidence and the change in the configuration static longitudinal and performance characteristics were then discussed in terms of these component lifts and their centers of pressure and angles of inclination. The purpose of this appendix is to describe the procedures used in computing the component lifts, pitching moments, and drag due to lift.

LIFT PREDICTION

The total lift on the configuration, exclusive of the camber effects, is assumed to be composed of the "body lift" and the "effective wing lift." The body lift is assumed to have a magnitude equal to the lift of the entire body alone and a location corresponding to the center of pressure of the entire body alone. The method of reference 7 was used for the computation of these body characteristics.

The effective wing lift is composed of the lift on an isolated wing formed by joining the two exposed wing panels, plus the interference lift on the exposed wing panel due to the presence of the body, and the interference lift on the body due to the exposed wing panels. The latter is included with the effective wing lift due to its dependence on wing lift. The centers of pressure of the isolated wing lift and both interference lifts are assumed to act at the same point, the center of area of the exposed wing panels. The two interference lifts are presented in reference 8 in terms of the lift-curve slope for the isolated wing, $(C_{L\alpha})_W$. As a result, the accuracy of the interference lift predictions depends on the accuracy with which $(C_{L\alpha})_W$ can be predicted. To avoid the inaccuracies associated with the prediction of this quantity by linear theory, the value of the wing alone lift-curve slope was obtained from the theoretical method of reference 8 with the aid of the experimental data. The theoretical relation between the lift variation with incidence and the wing alone lift-curve slope is given in reference 8 as:

$$k_{W(B)} + k_{B(W)} = \frac{[L_{W(B)} + L_{B(W)}] \text{ (due to } i_W)}{L_W} = \frac{(C_{L_{iw}})_{\alpha=0^0}}{(C_{L\alpha})_W} \qquad \text{(B1)}$$

where the quantities $k_{W(B)}$ and $k_{B(W)}$ are taken directly from reference 8 and $(C_{L_{iw}})_{\alpha=0^0}$ is the rate of change of lift coefficient with wing incidence at zero angle of attack.

The $C_{L_{i_W}}$ term was obtained from experimental data for the configuration with incidence angles of 0^0, -3^0 (modified body), and -6^0. (The addition of body volume under the wing to the -3^0 model is assumed to have no effect on lift at this angle of attack on the basis of comparable data for the -6^0 incidence model in figure 14.) This method derives an estimated wing-alone lift-curve slope. However, the assumptions used result in identical values for the predicted and experimental lifts at zero angle of attack. The wing-alone lift-curve slope derived from equation (B1) is compared in figure 7 with that predicted by linear theory. It is seen that at the higher Mach numbers an appreciable difference exists between the experimentally derived and theoretical lift-curve slopes.

The wing-alone lift-curve slope derived above, is also used as the basis for computing the interference lifts. The interference lift parameters are:

$K_{W(B)}-1$ interference effect on the wing due to the upwash induced along the wing span by the lifting body as the angle of attack is varied

$k_{W(B)}-1$ interference effect on the wing due to the intervening body which changes the original load distribution for the isolated wing formed by joining the two exposed wing panels, as the incidence angle is varied

$K_{B(W)}$ interference effect on the body due to carry-over of lift from a wing at angle of attack

$k_{B(W)}$ interference effect on the body due to carry-over of lift from a wing at angle of incidence

where k and K are the ratio of the lift component to the lift of the wing alone for variable wing incidence and variable angle of attack, respectively. The total interference lift at given angles of attack and incidence can be computed from:

$$C_{L_I} = \left\{ [K_{W(B)}-1]\alpha + [k_{W(B)}-1]i_w + K_{B(W)}\alpha + k_{B(W)}i_w \right\} C_{L_{\alpha_W}} \qquad (B2)$$

where the values of $K_{W(B)}$, $K_{B(W)}$, $k_{W(B)}$, and $k_{B(W)}$ are taken directly from reference 8.

The lift of the configuration can now be expressed as:

$$C_{L_C} = (C_{L_W} + C_{L_I}) + (C_{L_O})_{cam} + C_{L_B} \qquad (B3)$$

where the terms in the first parentheses represent the effective wing lift described above. The C_{L_B} term is calculated in reference 7. The $(C_{L_O})_{cam}$ term, which is taken as C_{N_O}, is given in the table of appendix A.

CENTER-OF-PRESSURE PREDICTION

The centers of pressure predicted by the method of reference 8 are tabulated below.

Lift parameter	Center-of-pressure location[1]			Assumed center-of-pressure location M = 3.0 - 5.0
	M = 3.0	M = 4.0	M = 5.0	
K_W	0.667	0.667	0.667	0.667
$K_{W(B)}$	.652	.652	.652	.667
$k_{W(B)}$	.668	.668	.668	.667
$K_{B(W)}$	.620	.640	.660	.667
$k_{B(W)}$	.620	.640	.660	.667

[1]Expressed in fractions of root chord of exposed wing.

It is seen that the centers of pressure of the interference lift as well as the centers of pressure of the wing alone are located near the center of area of the exposed wing panel, especially at the higher Mach numbers. This permits the combining of the wing-alone lift and all interference lifts into an effective wing lift which acts at the exposed wing center of area for moment computations.

The pitching-moment characteristics for the configuration, based on these assumptions, can be approximated at a given angle of attack by the sum of the following terms:

$$C_m = (C_{L_W} + C_{L_I})\frac{\bar{a}}{c_r} + C_{m_B} + (C_{m_0})_{cam} \tag{B4}$$

where

$C_{L_W} + C_{L_I}$ effective wing lift as derived in the previous section

$\dfrac{\bar{a}}{c_r}$ distance from moment center to exposed wing center of area expressed in fractions of root chord of total wing

C_{m_B} pitching moment of the body alone computed from the method of reference 7

$(C_{m_0})_{cam}$ experimental pitching moment due to camber at zero angle of attack

Some of the differences between experimental and predicted pitching-moment slopes for the 0° incidence model at Mach number of 3.0 (fig. 10) can be attributed to assuming the centers of pressure for $K_{B(W)}$ and $k_{B(W)}$ at a location different from that predicted in reference 8. There is a difference of 0.05 c_r between these two values. Since the $K_{B(W)}$ and $k_{B(W)}$ terms account for 70 percent of the interference lift for this particular case, the result is an error of 0.01 c_r. This discrepancy is not evident for the -6° incidence models as the $K_{B(W)}\alpha$ and $k_{B(W)}i_W$ terms of the lift equation (B2) are of opposite signs and tend to counteract each other.

DRAG DUE TO LIFT PREDICTION

In this report it was assumed that the drag due to lift of the configuration is determined by the inclinations of the component normal forces (ref. 2). The magnitudes of the component normal forces are equivalent to the magnitudes of the component lifts to the first-order degree of approximation. These component forces and their angles of inclination are:

1. The normal force of the exposed wing panels in the presence of the body, inclined to an angle of $\alpha + i_W$

2. The normal force of the body alone, inclined at an effective angle of $\alpha/2$ in accordance with slender-body theory

3. The interference normal force on the body in the presence of the wing, inclined to an angle of α

The drag-due-to-lift coefficient at a given angle of attack can then be expressed as:

$$C_{D(L)} = C_{L_{\alpha W}} \left\{ [K_{W(B)}\alpha + k_{W(B)}i_W](\alpha + i_W) + [K_{B(W)}\alpha + k_{B(W)}i_W](\alpha) \right\} +$$

$$(C_{L_B} \frac{a}{2}) \tag{B5}$$

and the total drag of a configuration utilizing incidence at a given angle of attack is:

$$C_{D_C} = C_{D_{\alpha=0}\circ} + C_{D(L)} + (C_{D_\alpha} + C_{N_O})\alpha_W \tag{B6}$$

where $C_{D_{\alpha=0}\circ}$ refers to the 0° incidence configuration at zero angle of attack. For the prediction of drag due to lift the theoretical values of $C_{L_{\alpha W}}$ and C_{L_B} and the various interference parameters described in the first portion of appendix B are used. For the total drag, the experimental values of C_{D_O} at Mach numbers from 3.0 to 5.0 and $(C_{A_\alpha})_{cam}$ at Mach numbers of 3.0 and 4.0 were used, as the interest lies in the prediction of drag changes due to incidence only. At a Mach number of 5.0, it was felt that the absolute magnitude of $(C_{A_\alpha})_{cam}$ was not representative because of the effect of boundary-layer transition movement on the body. However, the experimental increment between upright and inverted runs for the 0° incidence model agreed with the theoretical increment (fig. 16). This indicates that the theoretical value is of the correct magnitude for the case without boundary-layer transition and, as a result, the theoretical value of $(C_{A_\alpha})_{cam}$ was used at a Mach number of 5.0.

The invariance of the maximum lift-drag ratio with incidence can be explained in terms of the component lifts and their corresponding angles in equation (B5). Wing incidence results in a change of the zero-lift drag and a change in the drag due to lift from zero lift coefficient up to the lift coefficient for maximum lift-drag ratio. Zero lift for the -6° incidence configuration occurs at a finite positive angle of attack, where the positive body lift cancels the negative effective wing lift. The result is an increase in zero-lift drag due to the drag-due-to-lift terms of equation (B5). As the lift coefficient increases, the drag-due-to-lift variation with angle of attack can be obtained by differentiation of equation (B5)

$$C_{D_\alpha} = C_{L_{EW}} + \frac{1}{2} C_{L_B} \tag{B7}$$

where $C_{L_{EW}}$ is the effective wing lift coefficient which equals $(C_{L_W} + C_{L_I})$. The variation with incidence of the factors on the right

side of this equation can be seen in figure 8. The increase in the sum of $C_{L_{EW}}$ and C_{L_B} is approximately the same for the 0° and -6° incidence models from zero lift coefficient to the lift coefficient for maximum lift-drag ratio. It can also be seen that within this region of lift coefficients the ratio of body lift to effective wing lift is always larger for the -6° incidence model. As a result of the variations of these factors in the equation, it is seen that the increase in drag-due-to-lift from zero lift coefficient to that for maximum lift-drag ratio is smaller for the -6° incidence model. The absence of trim drag penalty for -6° of incidence can then be explained as a cancellation of the increase in zero-lift drag by a decrease in the drag due to lift.

A
2
2
4

REFERENCES

1. Nielsen, Jack N., Kaattari, George E., and Drake, William C.: Comparison Between Prediction and Experiment For All-Movable Wing and Body Combinations At Supersonic Speeds - Lift, Pitching Moment, and Hinge Moment. NACA RM A52D29, 1952.

2. Katzen, Elliott D., and Pitts, William C.: Comparison Between Prediction and Experiment For All-Movable Wing and Body Combinations At Supersonic Speeds - Drag Due to Lift and Lift-Drag Ratio. NACA RM A52I30, 1952.

3. Eggers, A. J., Jr. and Syvertson, Clarence A.: Aircraft Configurations Developing High Lift-Drag Ratios At High Supersonic Speeds. NACA RM A55L05, 1956.

4. Dennis, David H., and Petersen, Richard H.: Aerodynamic Performance and Static Stability at Mach Numbers up to 5 of Two Airplane Configurations With Favorable Lift Interference. NASA Memo 1-8-59A, 1959.

5. Eggers, A. J., Jr., and Nothwang, George J.: The Ames 10- by 14-Inch Supersonic Wind Tunnel. NACA TN 3095, 1954.

6. Puckett, Allen E.: Supersonic Wave Drag of Thin Airfoils. Jour. Aero. Sci., vol. 13, no. 9, Sept. 1946, pp. 475-484.

7. Allen, H. Julian: Estimation of the Forces and Moments Acting on Inclined Bodies of Revolution of High Fineness Ratio. NACA RM A9I26, 1949.

8. Pitts, William C., Nielsen, Jack N., and Kaattari, George E.: Lift and Center of Pressure of Wing-Body-Tail Combinations at Subsonic, Transonic, and Supersonic Speeds. NACA Rep. 1307, 1957.

A
2
2
4

DECLASSIFIED

A
2
2
4

C_r

Fuselage

Length = 9.50 in.
Base diameter = 0.95 in.
Volume = 3.37 in.^{3}
Shape: 1/2-power body of revolution
($r = .154 \times ^{1/2}$)

Wing

Incidence = 0°
Leading-edge sweep = 70°
Trailing-edge sweep = 0°
Aspect ratio = 1.45
Span = 4.66 in.
Root chord = 6.40 in.
Area = 14.92 in.^{2}
Airfoil:

0.025 C

0.5 C

C
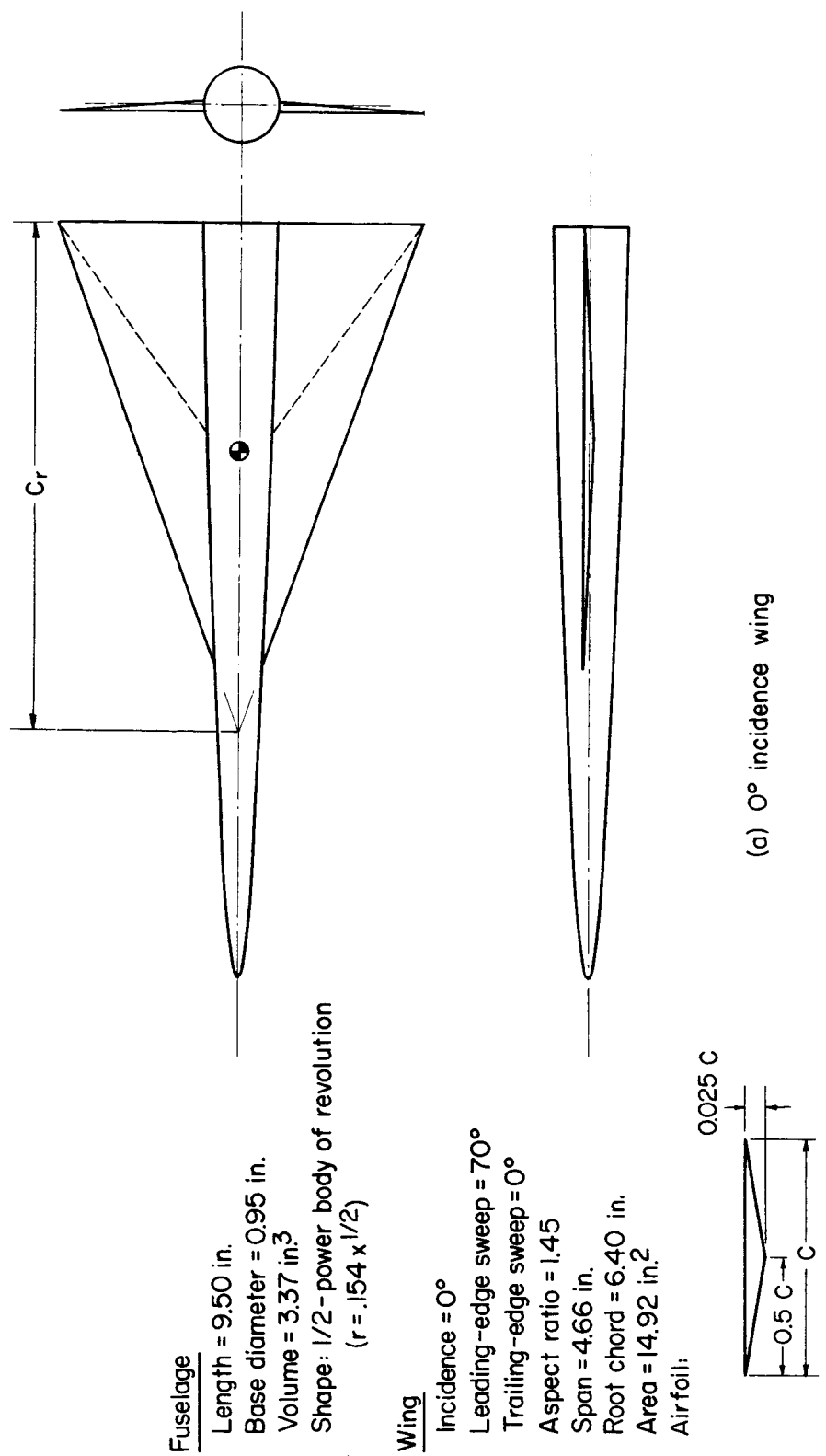
(a) 0° incidence wing

Figure 1.- Test models.

26
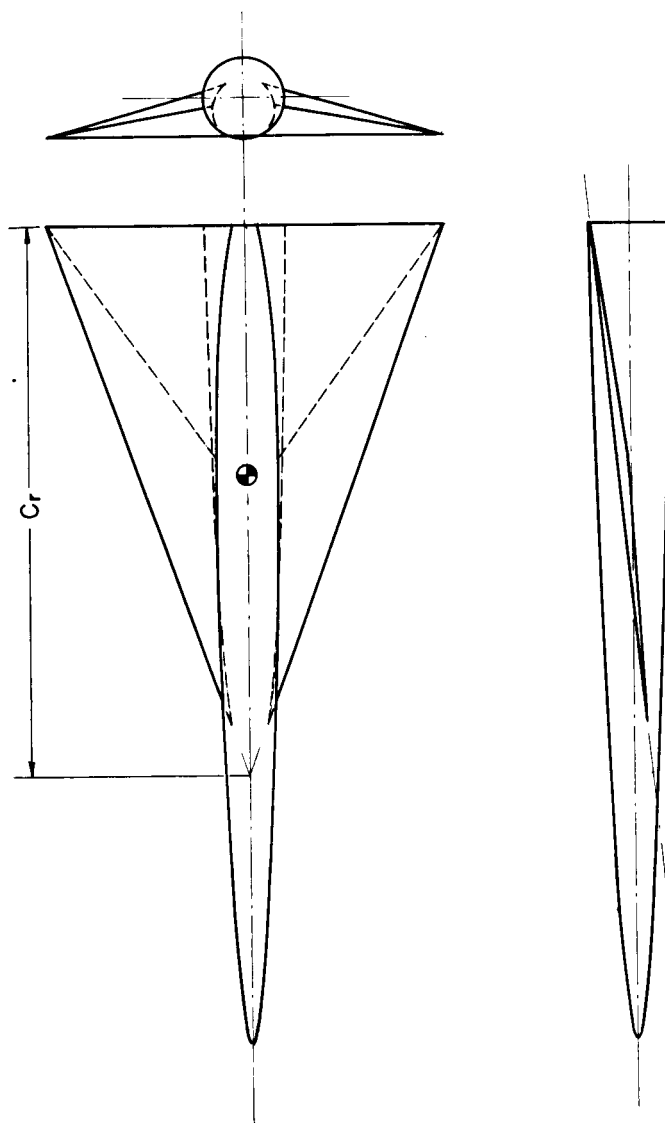
(b) -6° incidence wing

Figure 1.- Continued.

A
2
2
4

A
2
2
4

C_r

A

A

Added volume

A-A
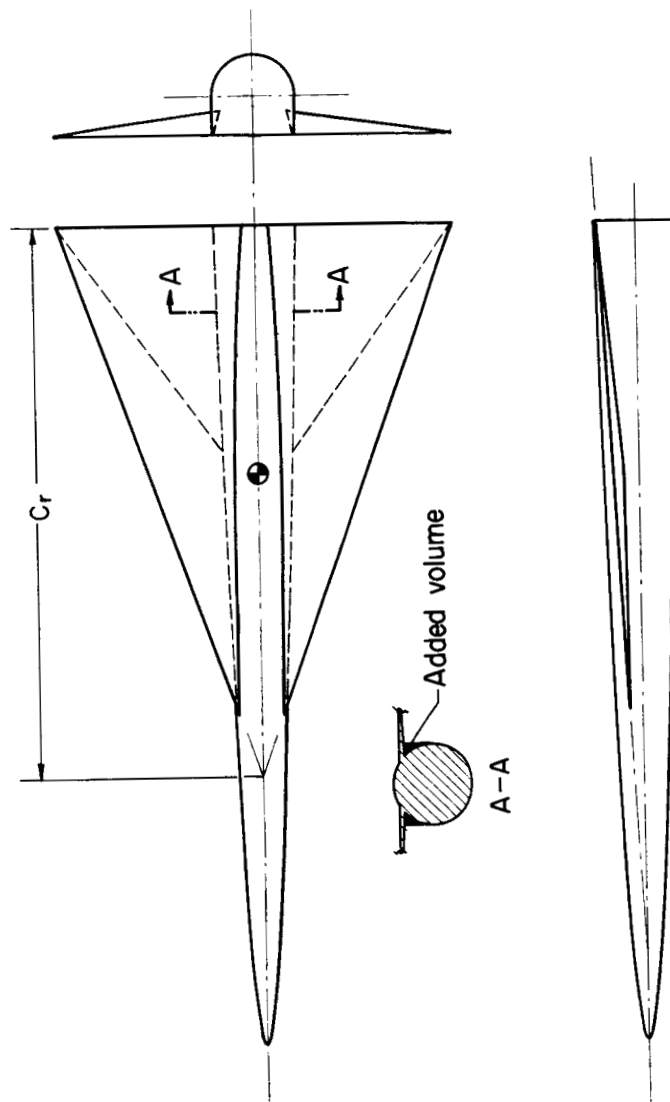
(c) -3° incidence wing on modified body

Figure 1.- Continued.
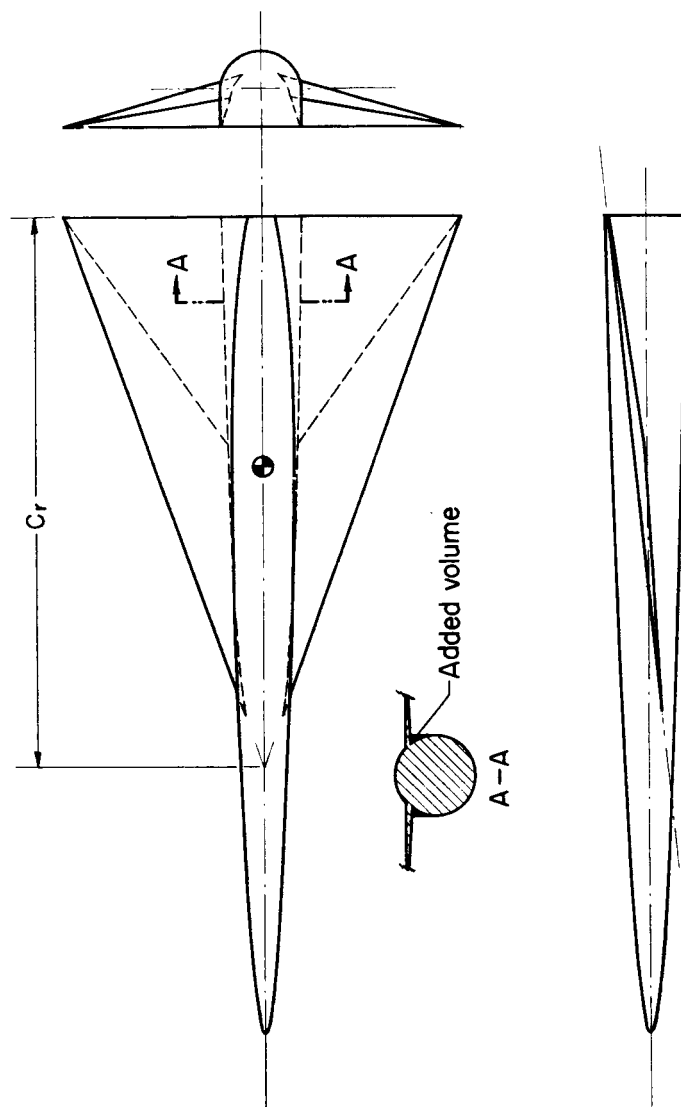
(d) –6° incidence wing on modified body

Figure 1.– Concluded.
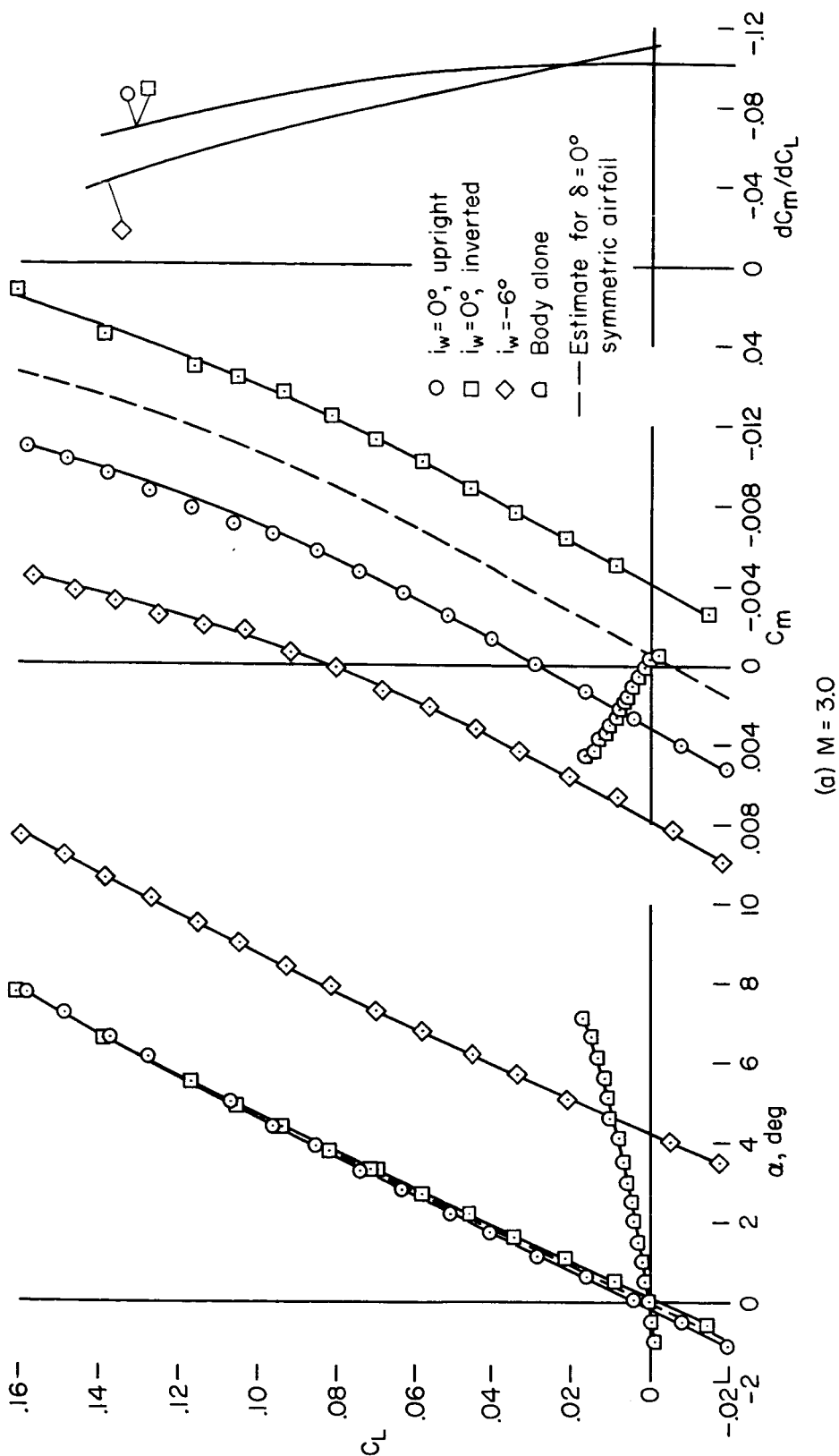
Figure 2.- Longitudinal characteristics of test models with symmetrical body.

(a) M = 3.0

○ $i_w = 0°$, upright
□ $i_w = 0°$, inverted
◇ $i_w = -6°$
◻ Body alone
—— Estimate for $\delta = 0°$ symmetric airfoil

A
2
2
4

(b) M = 4.0

Figure 2.- Continued.

○ $i_w = 0°$, upright
□ $i_w = 0°$, inverted
◇ $i_w = -6°$
◌ Body alone
—— Estimate for $\delta = 0°$ symmetric airfoil
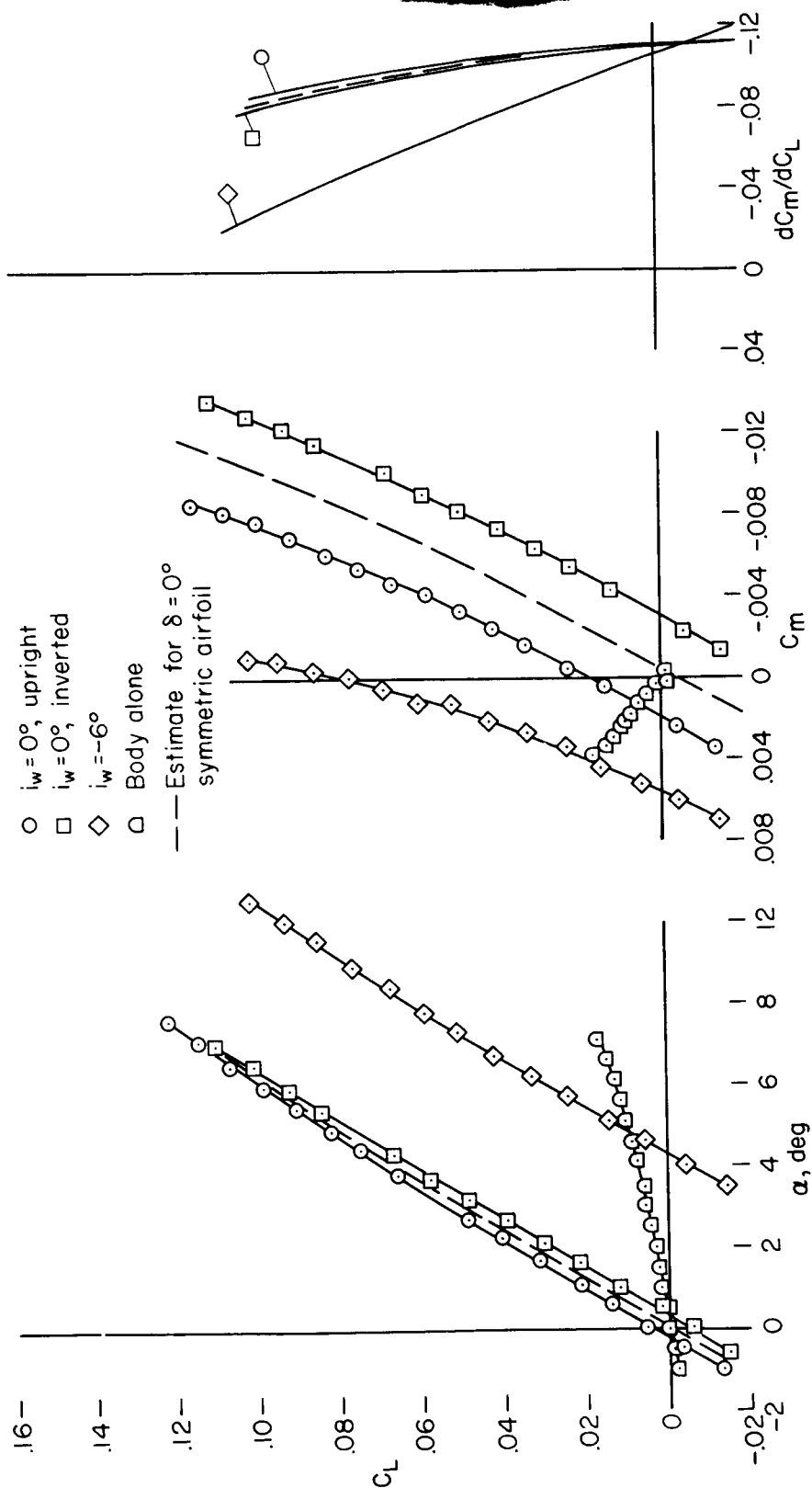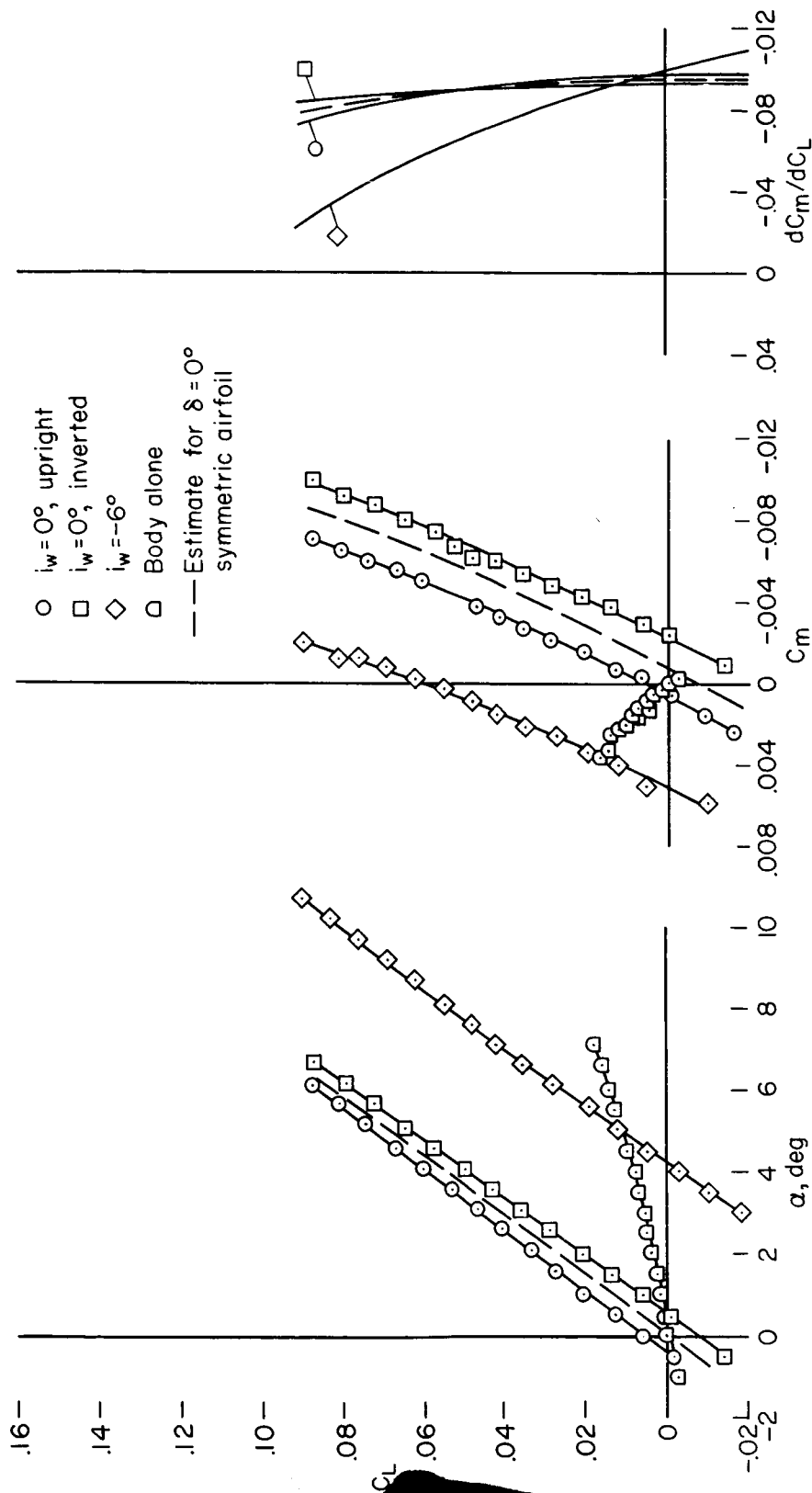
(c) M = 5.0
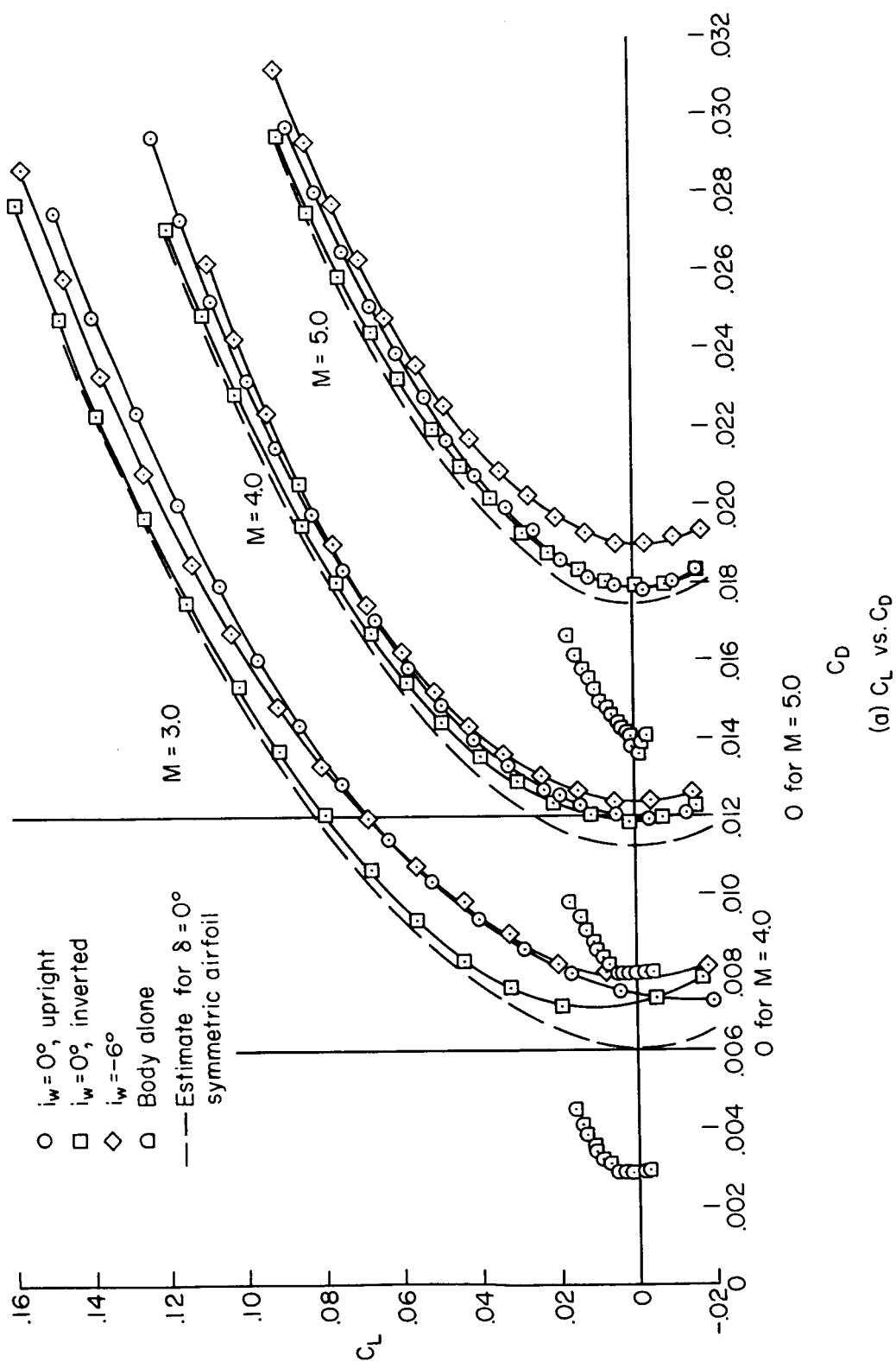
Figure 2.- Concluded.

Figure 3.- Performance characteristics of test models with symmetrical body.

(a) C_L vs. C_D

(b) L/D vs. C_L
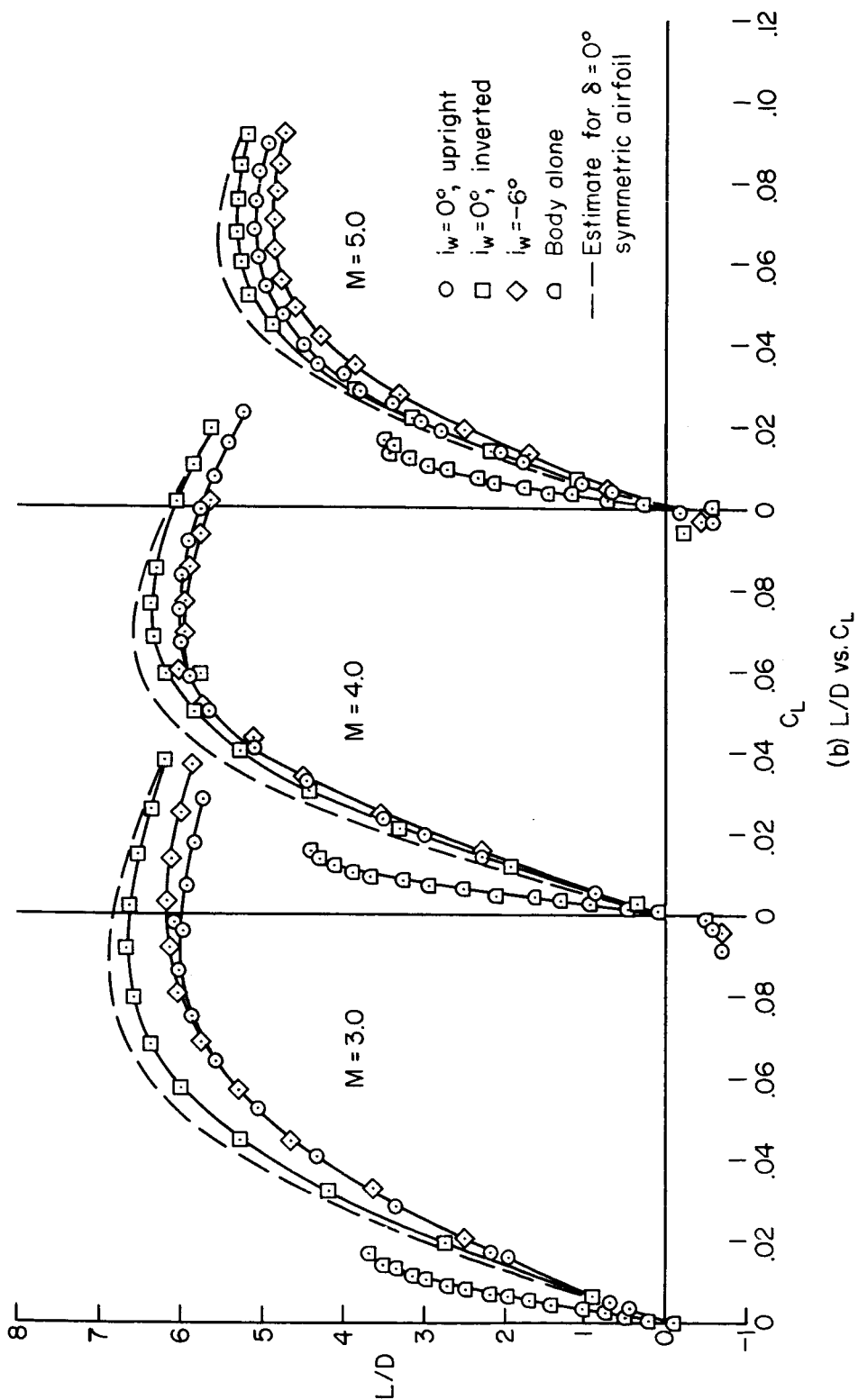
Figure 3.- Concluded.
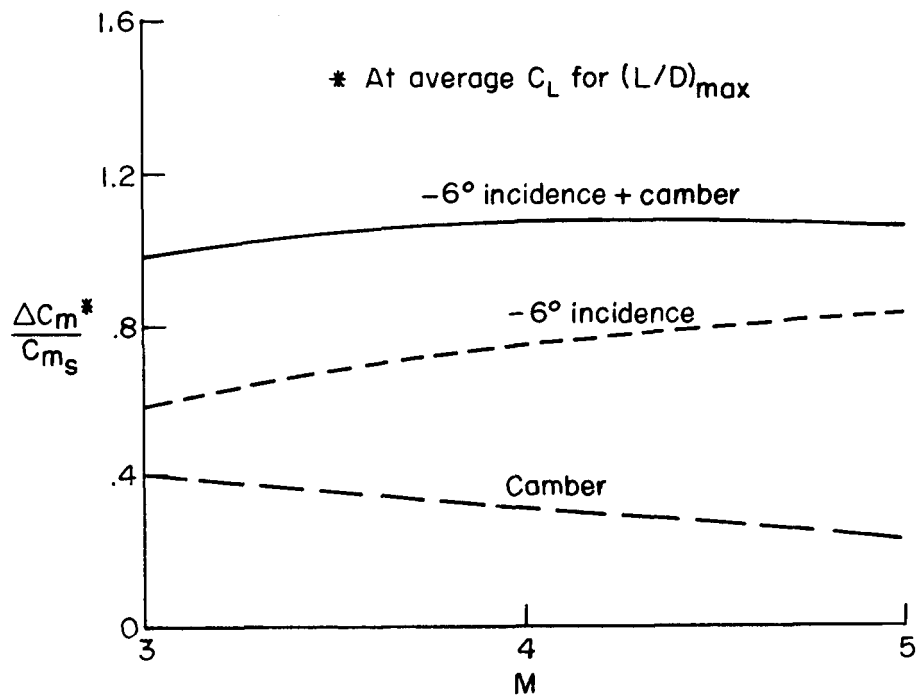
Figure 4.- Incremental pitching moment due to camber and incidence.

A
2
2
4
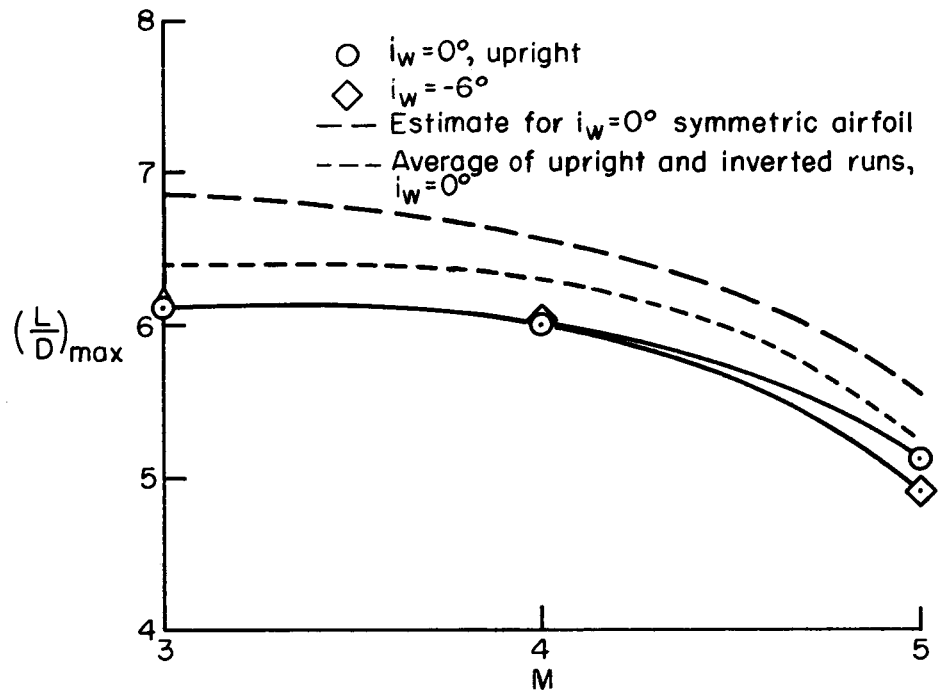
Figure 5.- Effect of camber and incidence on lift-drag ratio.
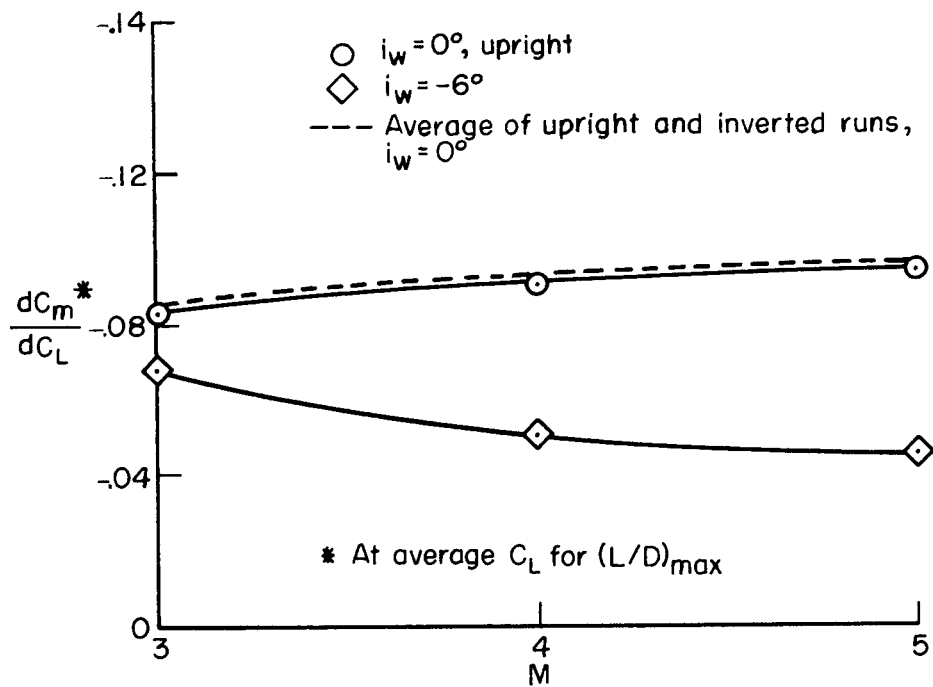
Figure 6.- Effect of camber and incidence on static longitudinal stability.

A
2
2
4
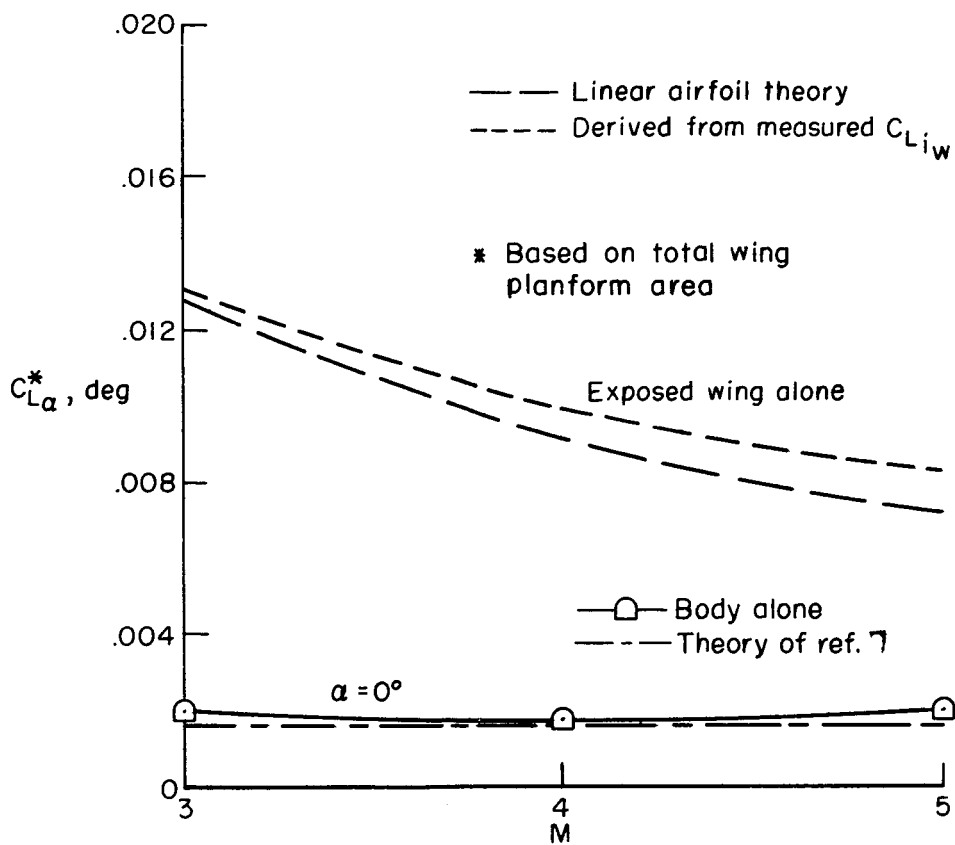
Figure 7.- Variation with Mach number of estimated and measured lift-curve slopes.
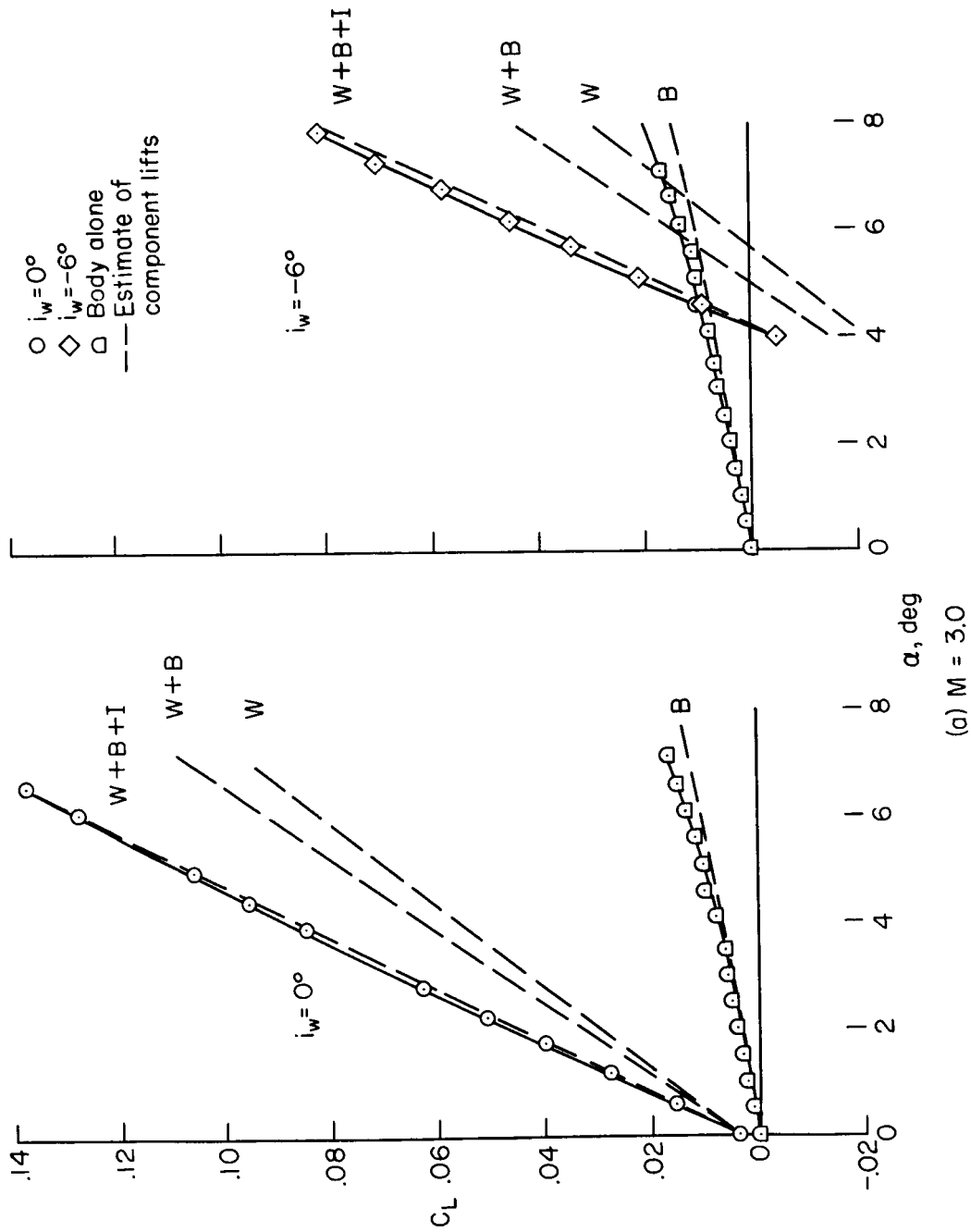
Figure 8.- Comparison of estimated and measured lift characteristics.
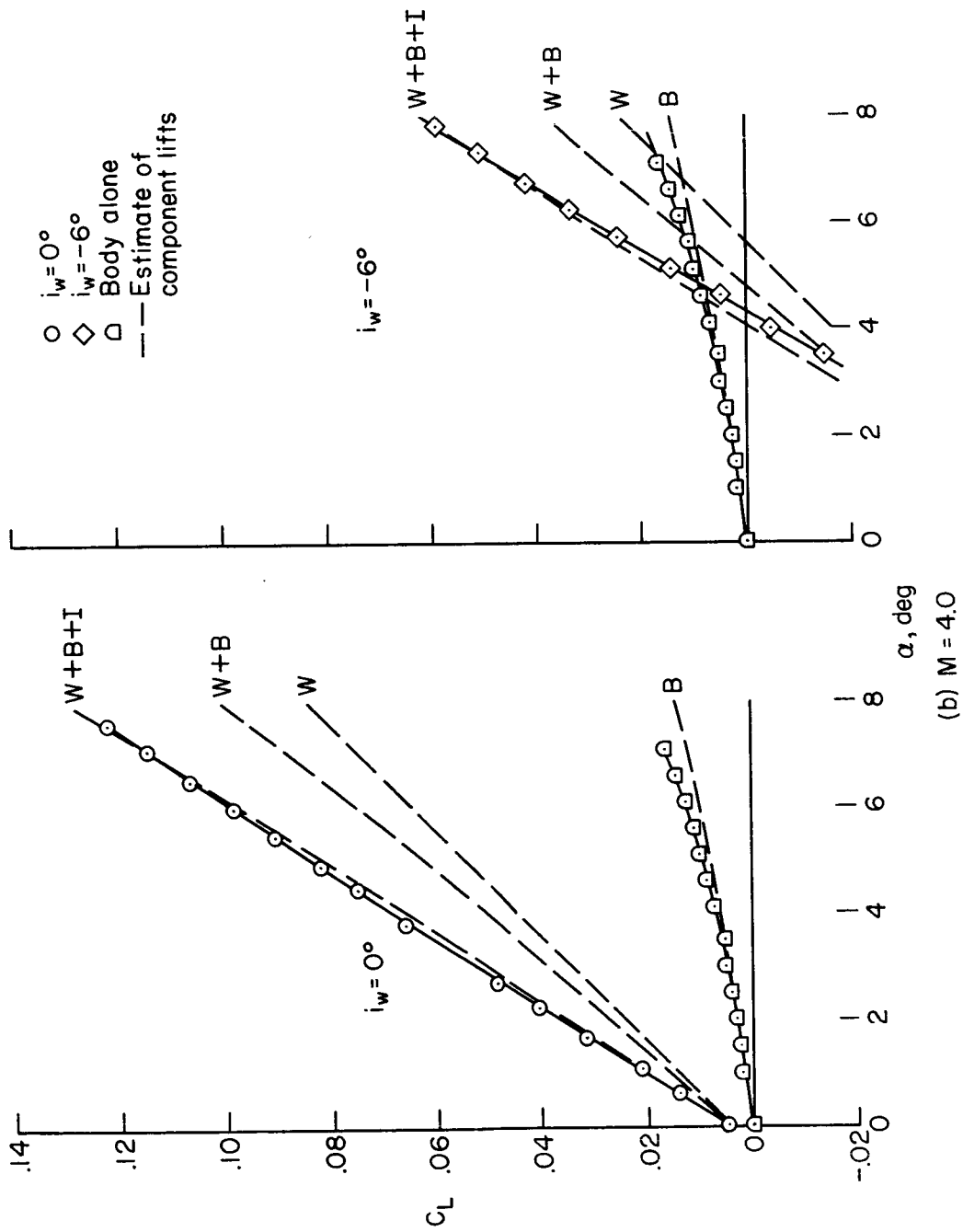
(a) M = 3.0

(b) M = 4.0

Figure 8.- Continued.
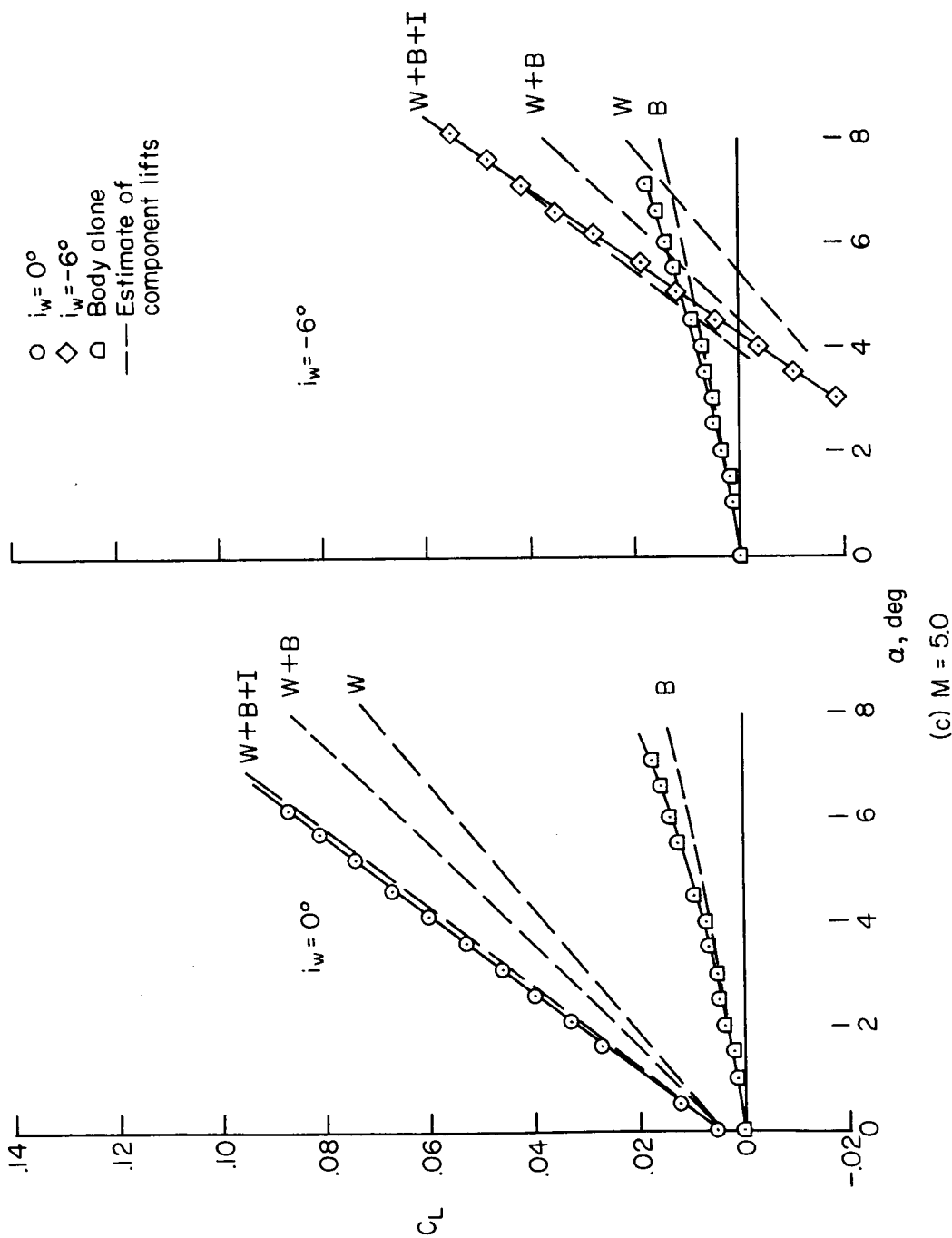
(c) M = 5.0

Figure 8.- Concluded.

A
2
2
4

A
2
2
4
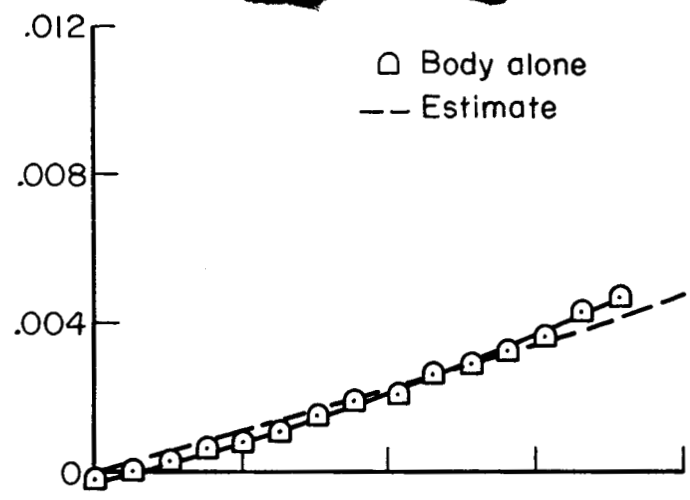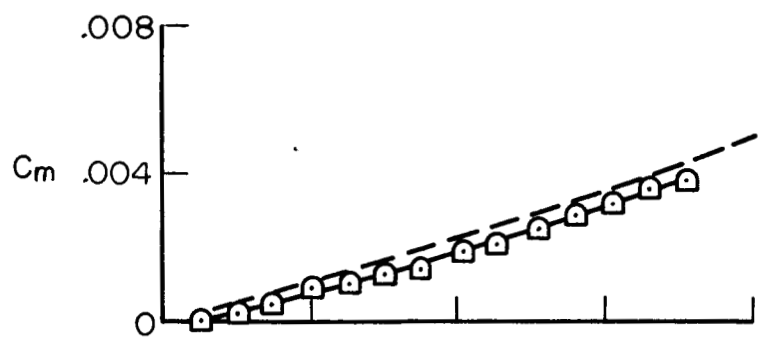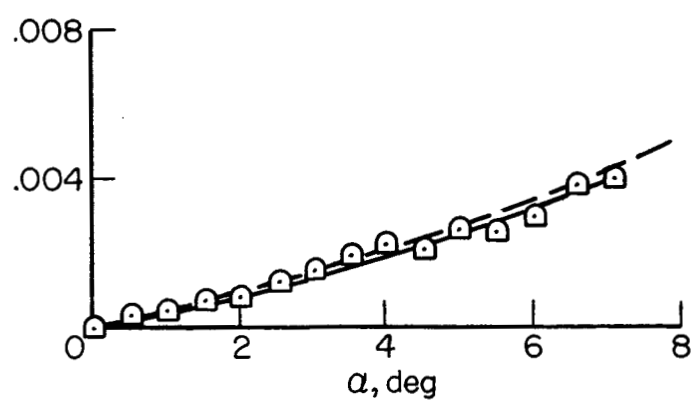
(a) M = 3.0

(b) M = 4.0

(c) M = 5.0

Figure 9.- Comparison of estimated and measured pitching-moment characteristics for the body alone.
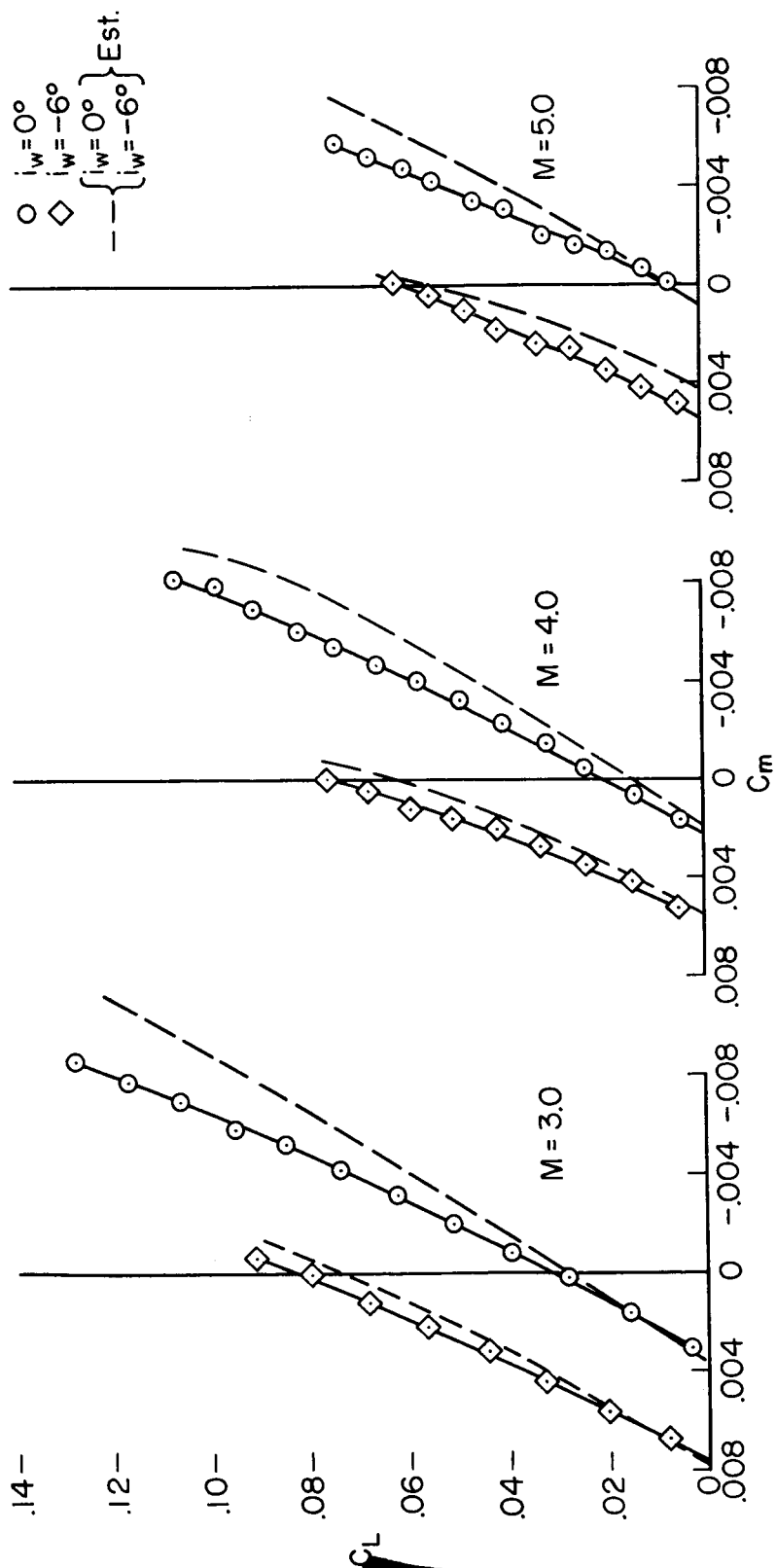
Figure 10.- Comparison of estimated and measured pitching-moment characteristics.
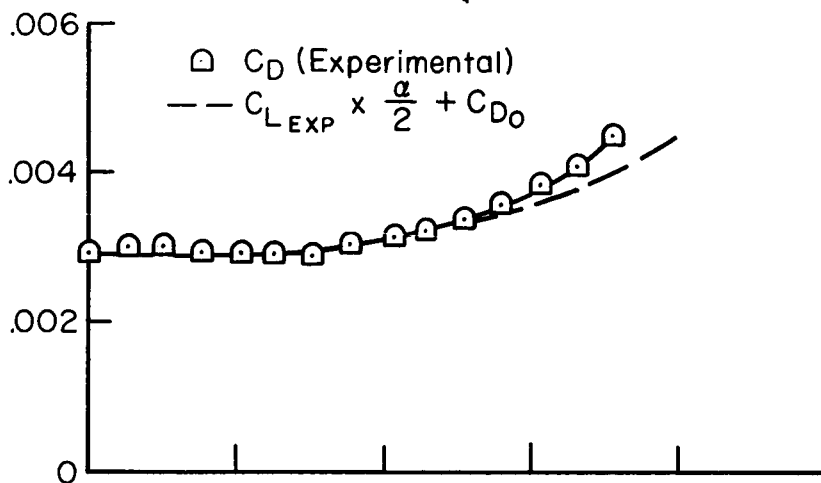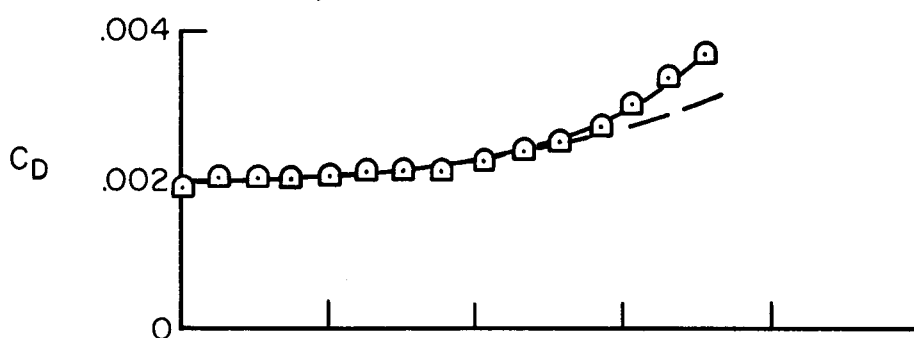
(a) M = 3.0

(b) M = 4.0
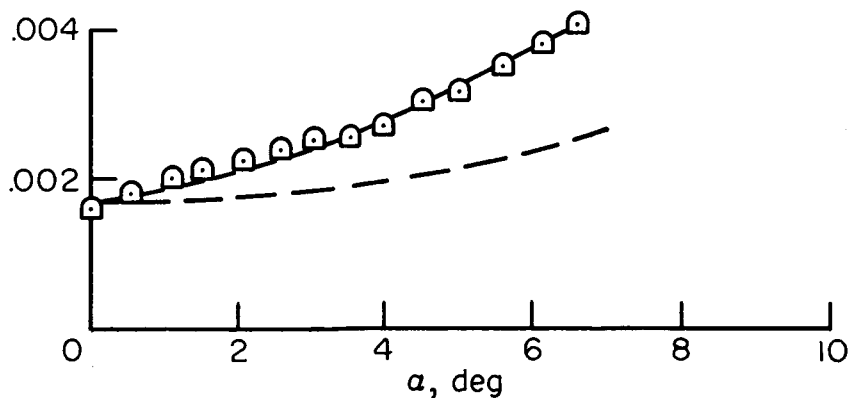
(c) M = 5.0

Figure 11.- Estimated and measured variation of body alone drag with angle of attack.
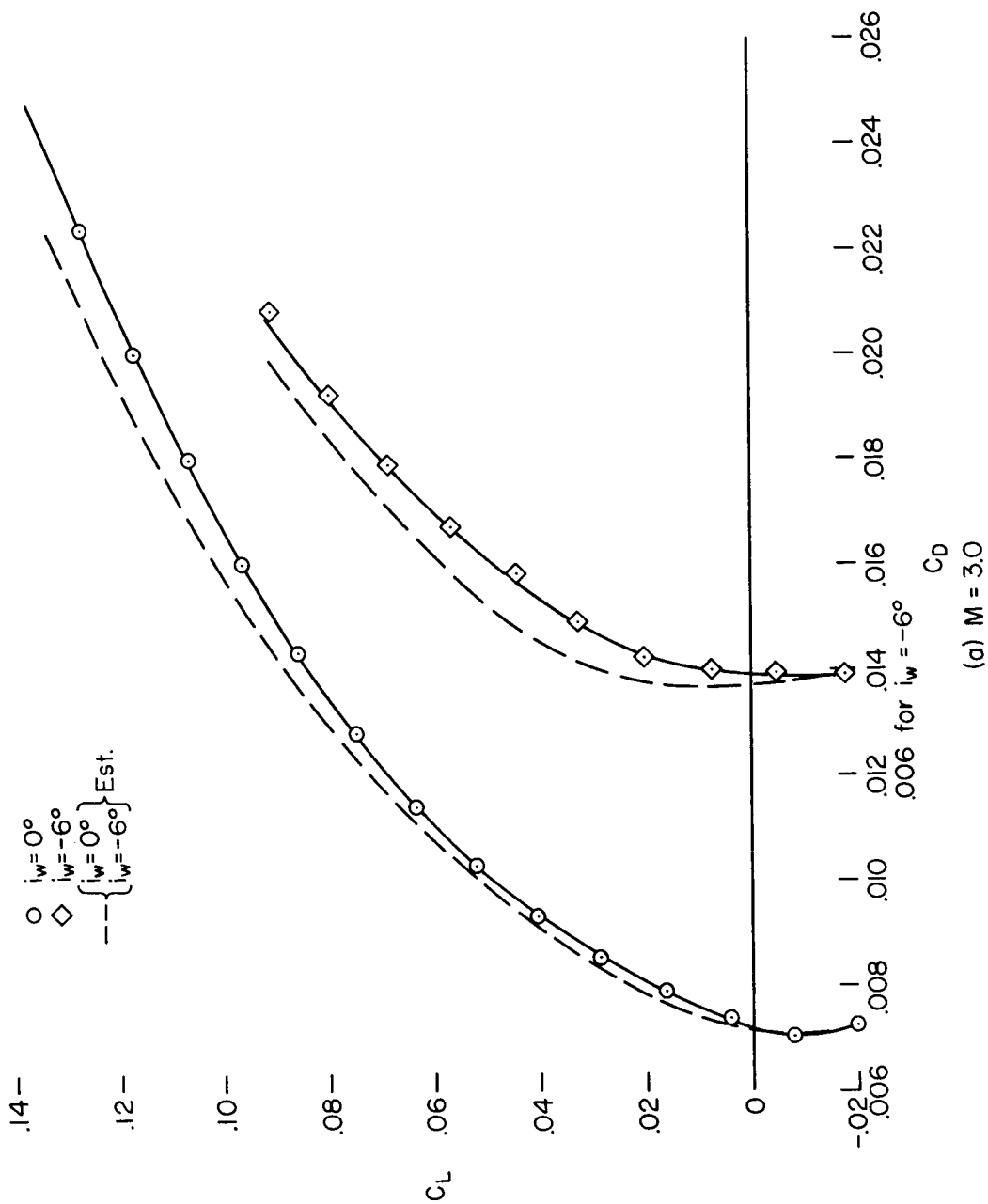
Figure 12.- Comparison of estimated and measured drag due to lift characteristics.

(a) M = 3.0

(b) M = 4.0

Figure 12.- Continued.

(c) M = 5.0

Figure 12.- Concluded.

C_{Y_β}

-.008

-.004

0

C_{n_β}

-.0008

-.0004

0

C_{l_β}

-.0012

-.0008

-.0004

0

$\bigcirc\ i_w = 0°,$ upright
$\triangle\ i_w = -3°,$ modified
$\triangle\ i_w = -6°,$ modified

-4 0 4 8

(a) M = 3.0

(b) M = 4.0

(c) M = 5.0

α, deg
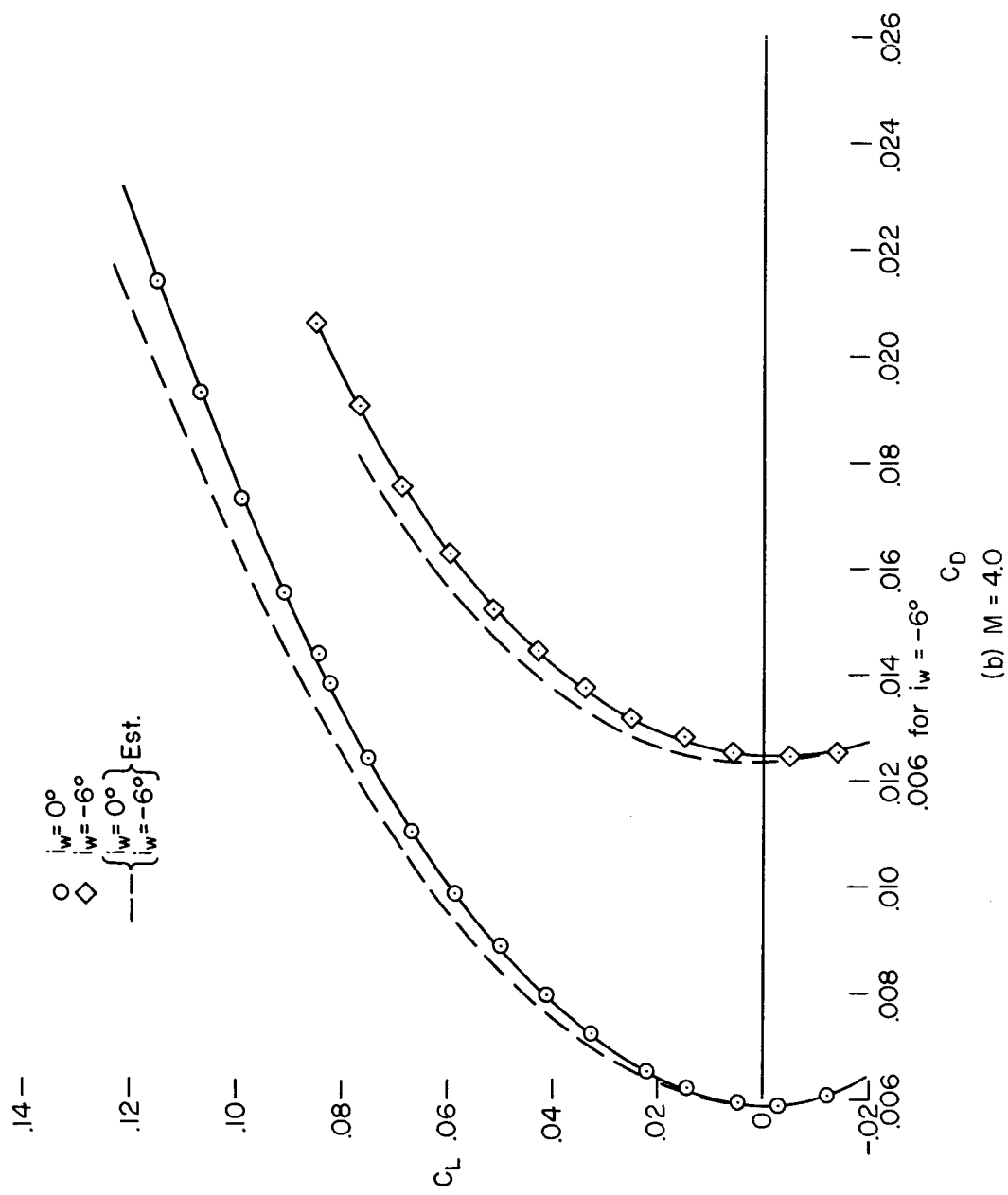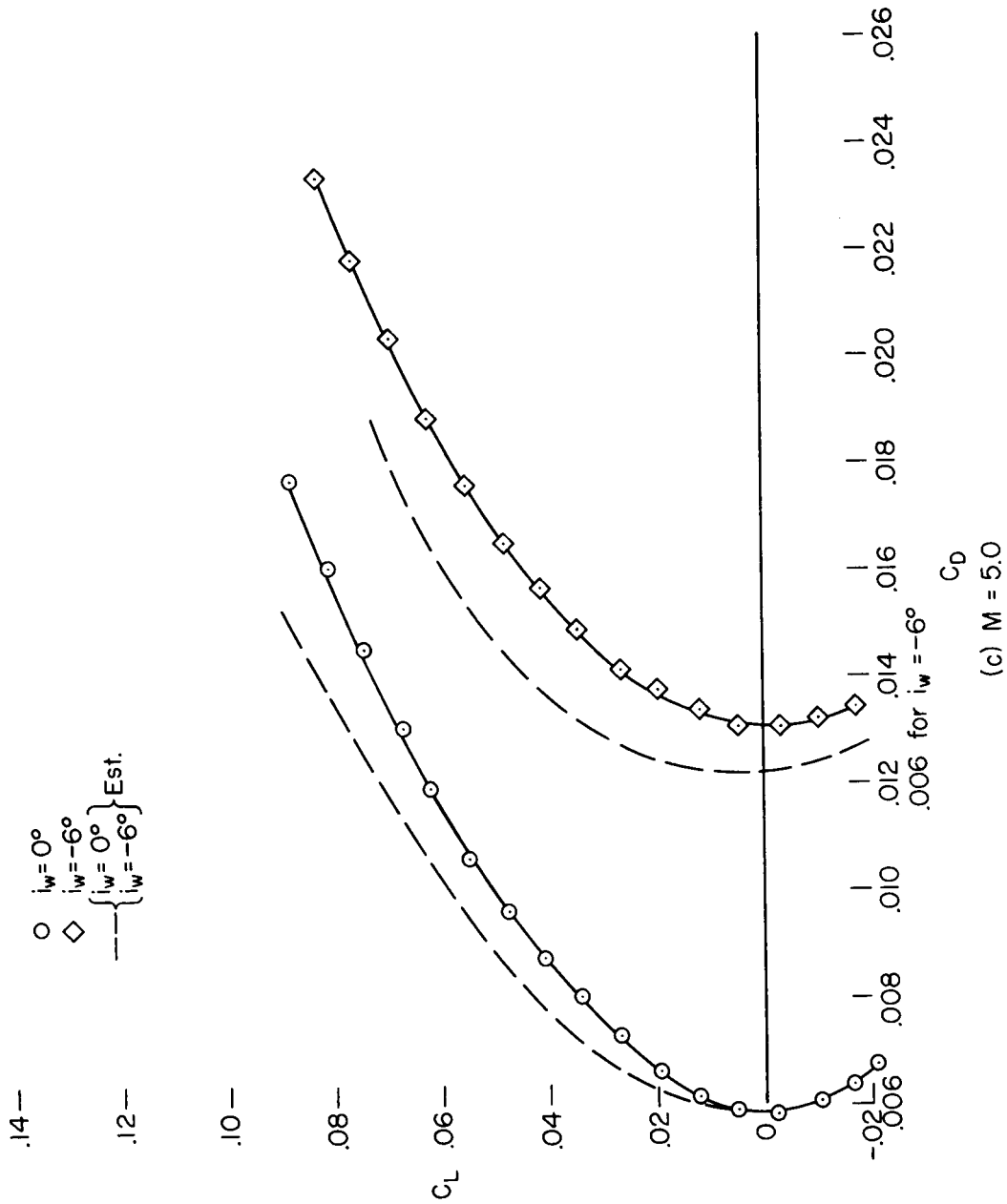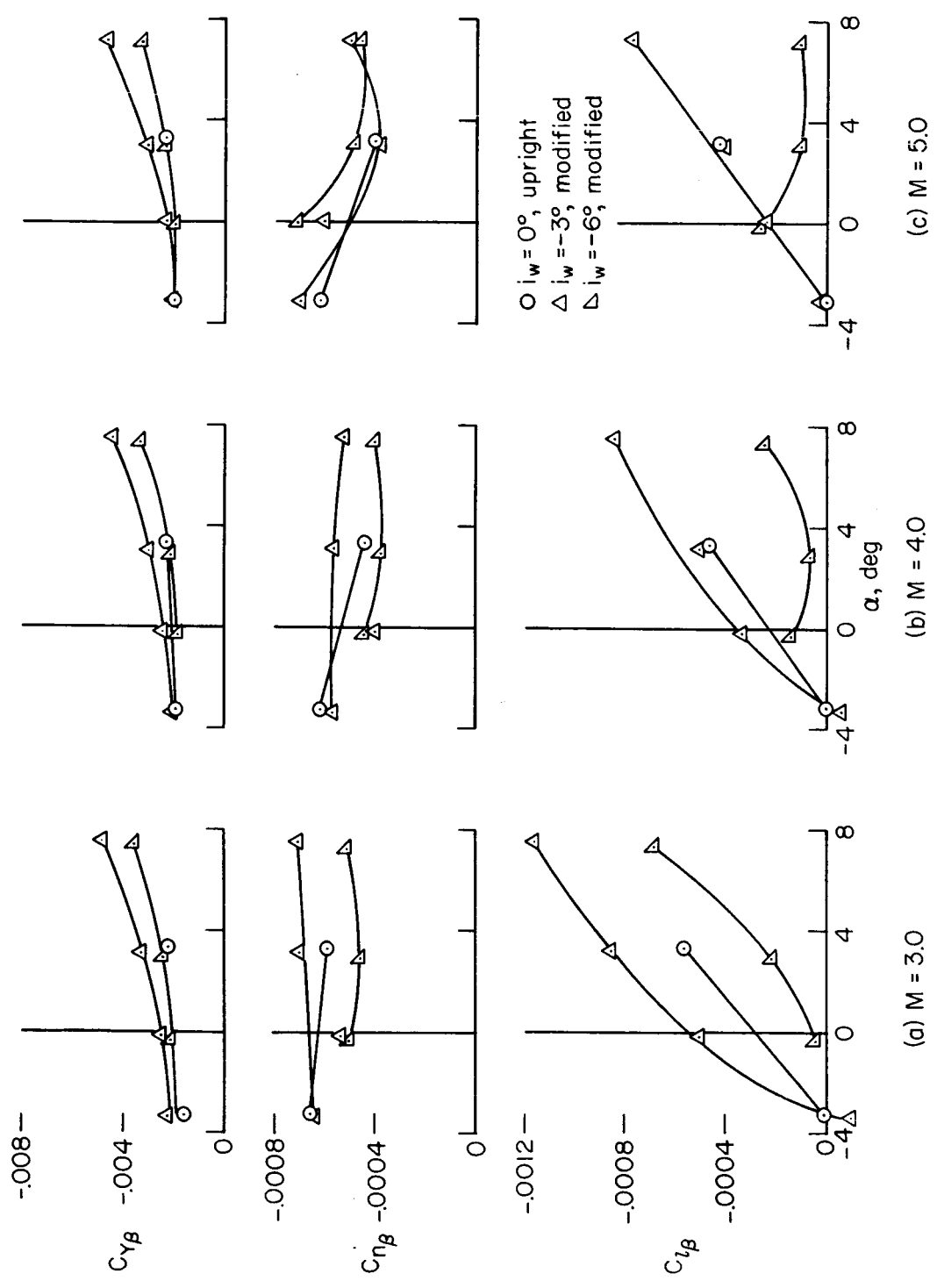
Figure 13.- Measured lateral-directional static derivatives.
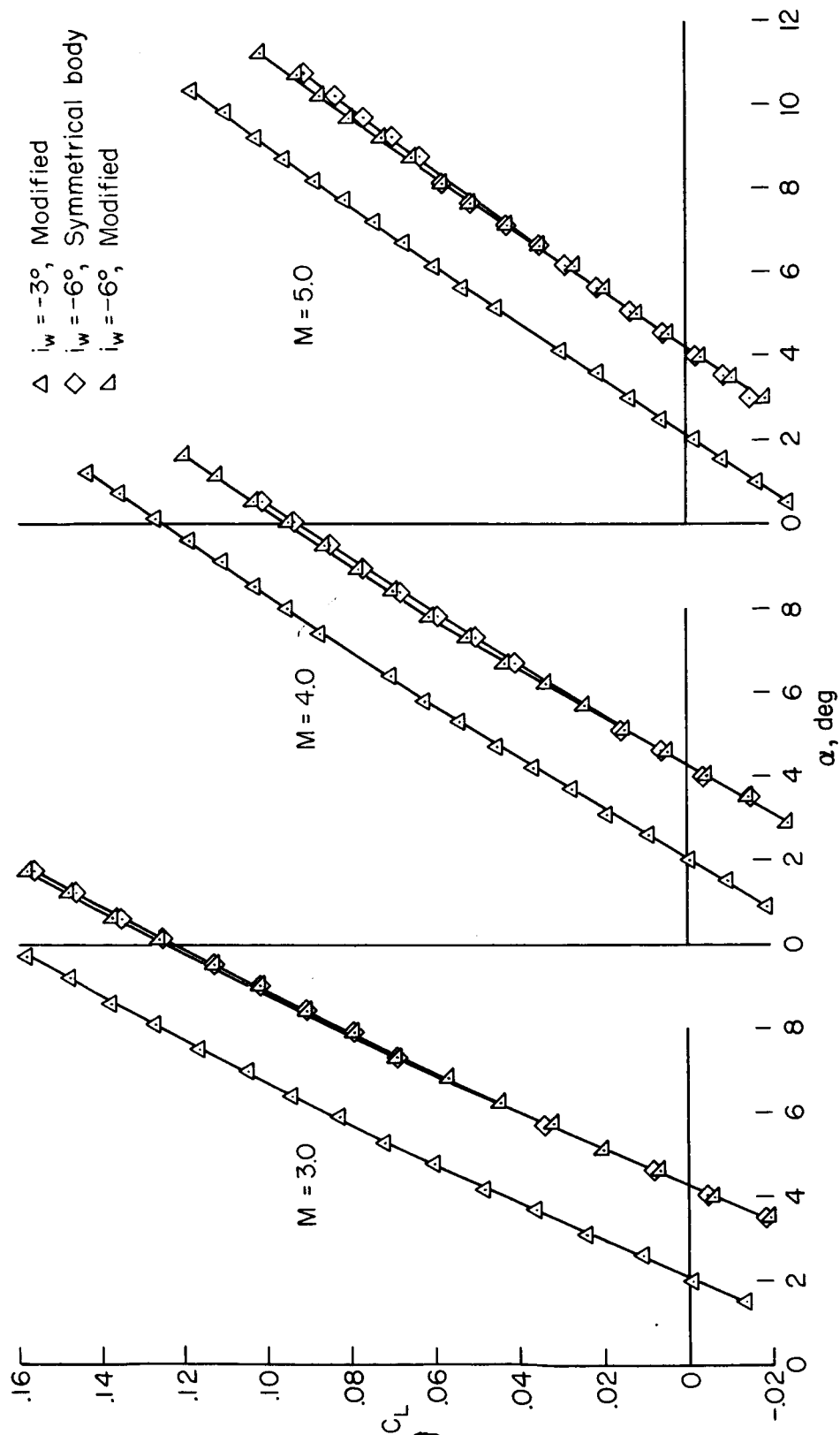
(a) C_L vs. α

Figure 14.- Effect of fuselage modification on longitudinal characteristics.

A 424

△	$i_w = -3°$, Modified
◇	$i_w = -6°$, Symmetrical body
△	$i_w = -6°$, Modified

M = 5.0

M = 4.0

M = 3.0

C_m
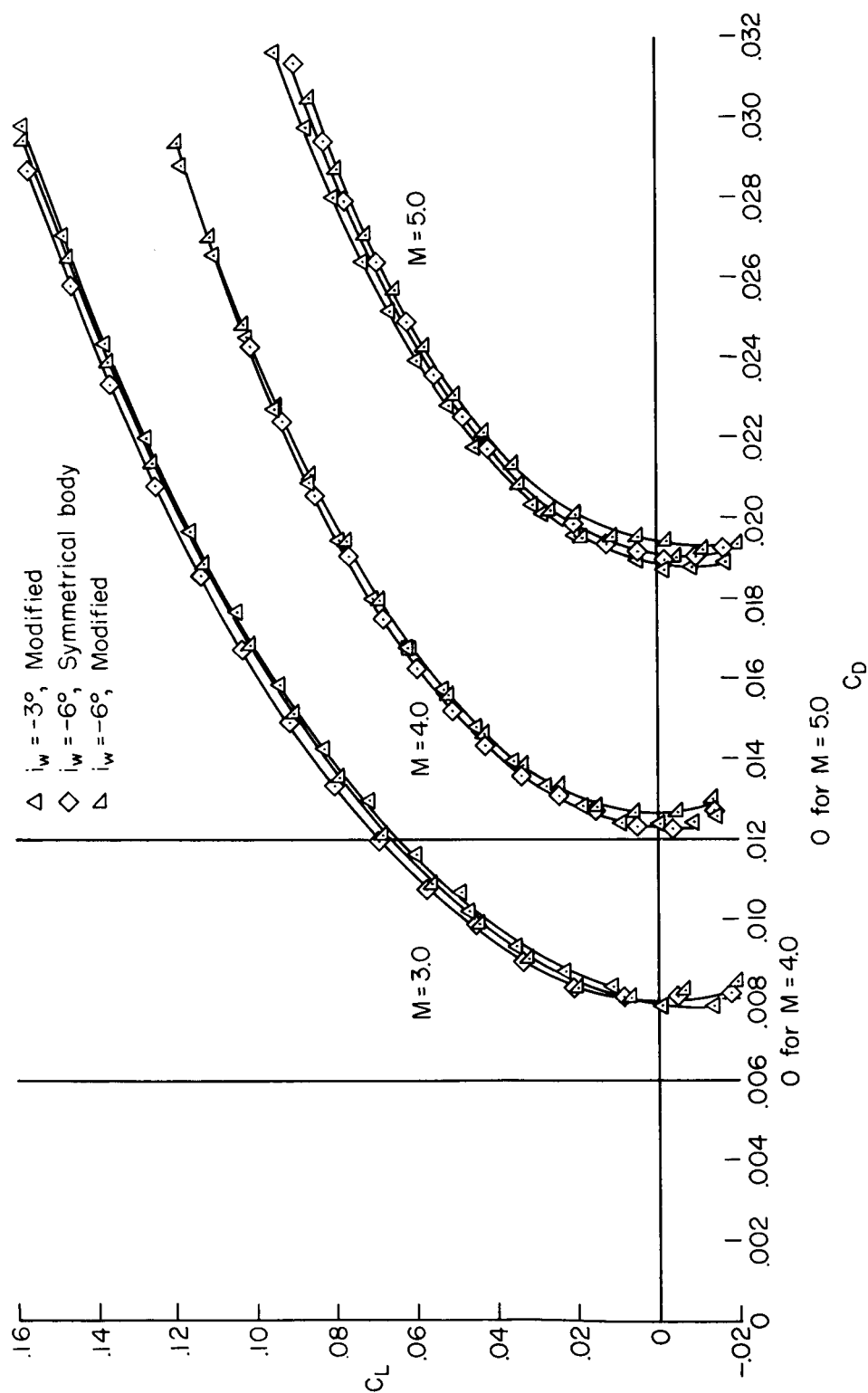
C_L
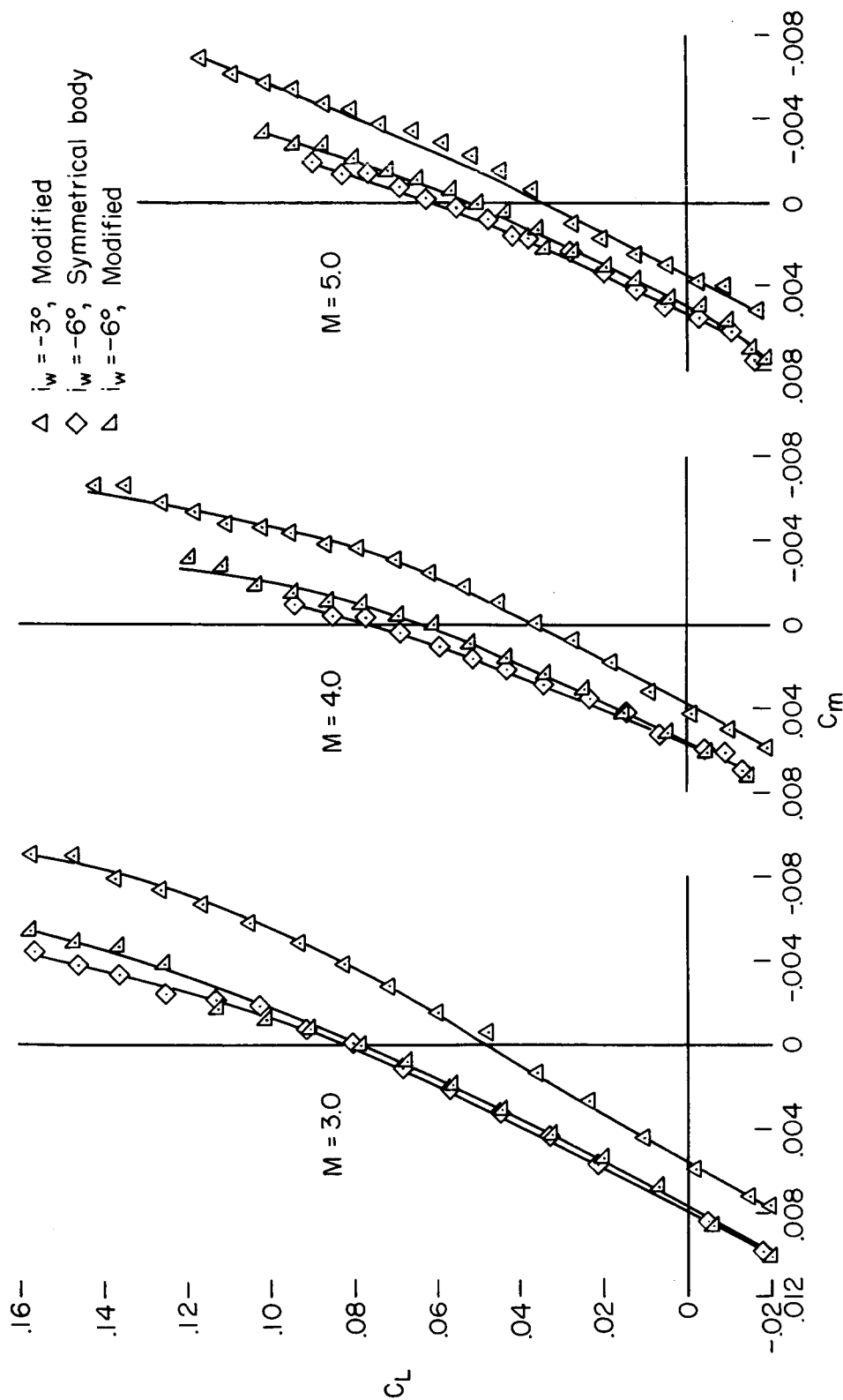
(b) C_L vs. C_m

Figure 14.- Concluded.

(a) C_L vs. C_D

Figure 15.- Effect of fuselage modification on performance characteristics.
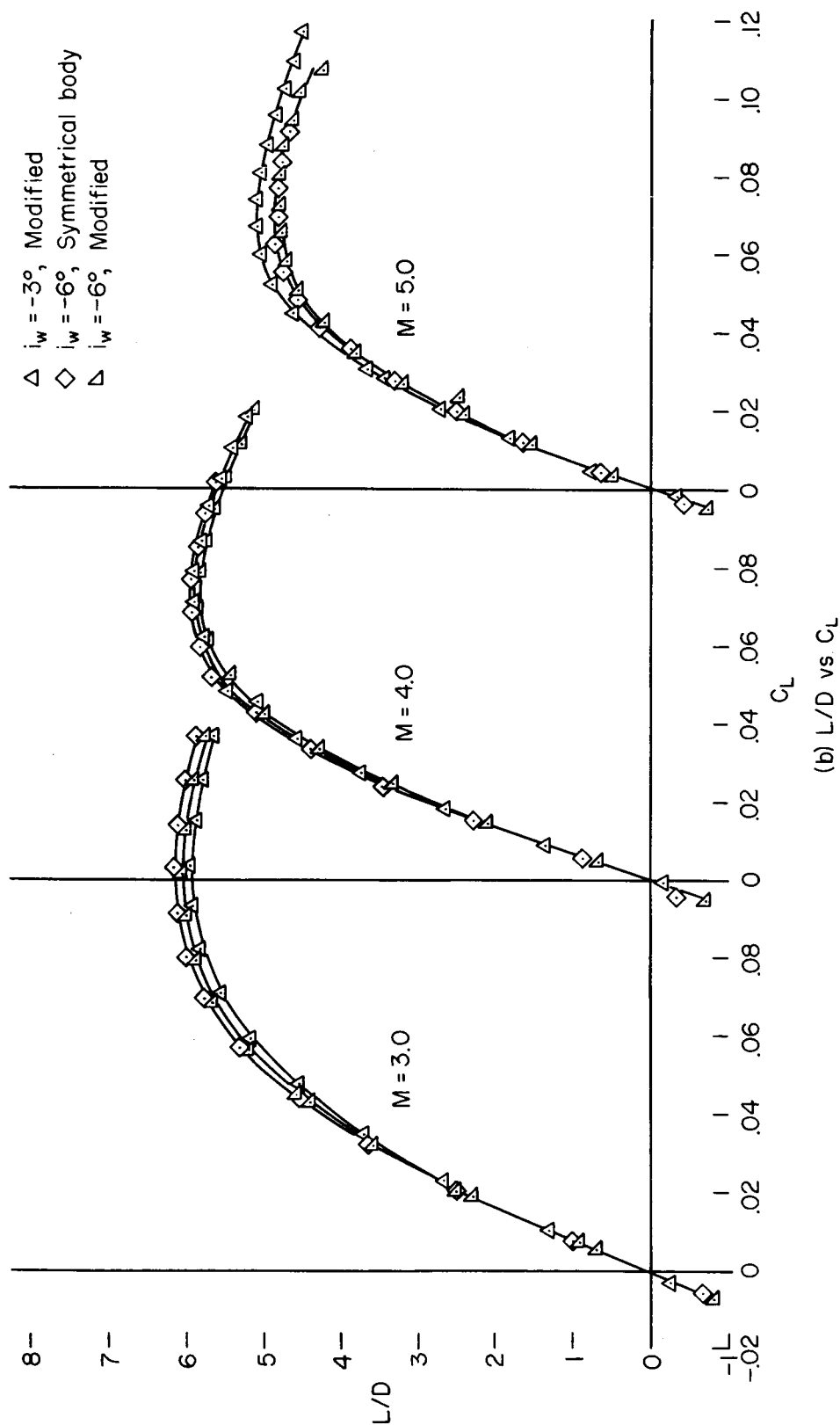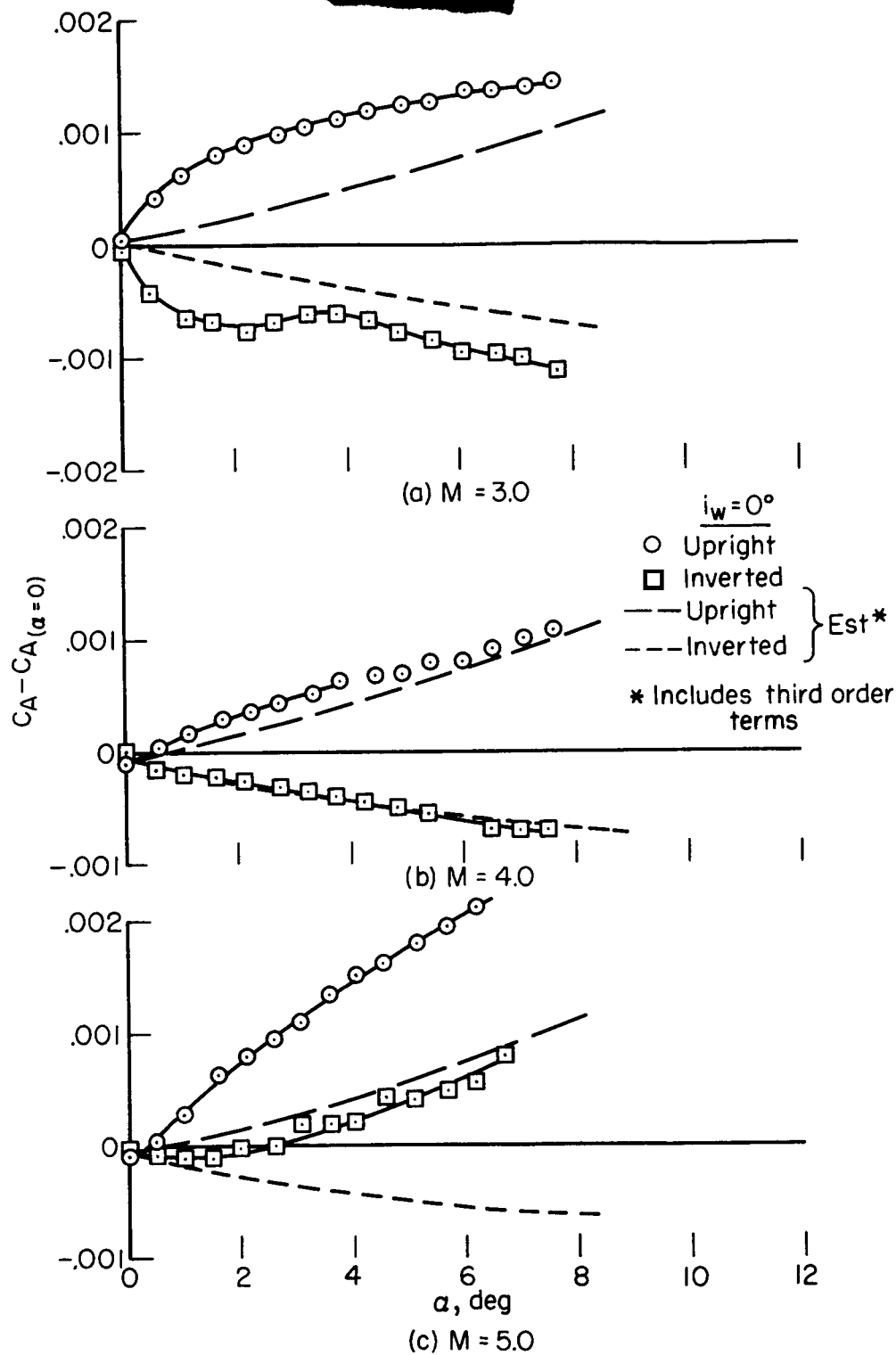
(b) L/D vs C_L

Figure 15.- Concluded.

Figure 16.- Variation of axial force with angle of attack.